Scuola Internazionale Superiore di Studi Avanzati

International School for Advanced Studies

Bond Particle Model for Semiconductor Melts : Application to the liquid Structure of Germanium and Analysis of supercooled States

Thesis submitted for the degree of

"Magister Philosophiæ"

CANDIDATE

Andrea Ferrante

SUPERVISOR

Prof. Mario P. Tosi

Academic year 1989/90

Chapter 1

Introduction and overview

Simple models of interatomic forces have had an important role in advancing qualitative and quantitative understanding of condensed matter. In relation to properties of the liquid state, the fluids of neutral and charged hard spheres, the classical one-component plasma and the Lennard-Jones fluid have played such a role under two main aspects. Not only do they mimic classes of real fluids, but also provide simple test models for progress in statistical mechanics through joint theoretical and computer simulation studies.
Bond directionality and association are qualitative features of many real systems which are missing in the models mentioned before. One can ask whether models of the same simplicity can be developed to describe structural properties of the disordered phases for system in which covalent bonds play a major role.

Scope of this thesis is to illustrate a simple primitive model for a liquid, that shows both strong directional interactions and a variable degree of association in the liquid phase, model which is relevant for the study of the disordered phases of IV group elemental and III-V compound semiconductors.

A considerable interest from both the theoretical and experimental point of view has been devoted in recent years to the study of the structure of covalently bonded systems in disordered states. A first class of systems extensively investigated is that constituted by a a number of ionic or semiconducting compound materials of type AX_2 that share the common properties to be well- known glass formers: among them[1,2] BeF_2, $ZnCl_2$, GeO_2, SiO_2, $GeSe_2$, $SiSe_2$. On cooling

from the melt at relatively moderate quench-rates, they can form a network-glass, that is an open structure with tetrahedral local coordination around the A atom, which is stabilized by the presence of strong directional interaction. As a matter of fact all these compounds are known to form covalent bonds of more or less ionic character, that lead in the crystalline state to the formation of tetrahedral units of X atoms coordinated to one A atom. Such fourfold coordination can successfully be distinguished from others in the crystal structure classification built by Andreoni[3] for AX_2 compounds on the basis of quantal parameters of the component elements. The tetrahedral units can form an extended structure by connecting either by corner sharing or by edge sharing. This leads in the crystal state to the formation of 1D, 2D, or 3D regular networks respectively in the case of $SiSe_2$ (pure edge sharing), $GeSe_2$ (mixed edge and corner sharing), SiO_2 (pure corner sharing), and various allotropic crystalline forms distinguished by their medium range topology may also exist for a given compound (i.e. SiO_2). The glassy structure can be viewed as a disordered network of distorted tetrahedra, and an important point for its characterization is to understand how this units connect together to form an extended network, and what is the medium range topology that arises by their correlation. Interesting structural questions thus concern, the relative weight of corner and edge sharing, the "ring" statistics, and the presence of residual traces of low network dimensionality. From the experimental point of view the structure of the vitreous or amorphous state is reflected not only in static properties determined by elastic scattering experiments, but also in inelastic neutron scattering spectra[4] , as well as in Raman scattering spectra[5]. As the information is not sufficient to fully characterize the structure as in the crystal states, models have been used to translate experimental results in structural terms.

The medium range order in the these glasses is characterized by the presence

of a first sharp diffraction peak (FSDP) in S(k) in the range from 1.0 to 1.5 $\AA^{-1}$, that arises from the connectivity of tetrahedral units in the network[2].

The corresponding liquids near melting (and in the supercooled states preceding the glass transition) is thought to show also a "network- like" structure, in the sense that a quite high degree of association between A and X atom is present due to strong directional interactions, leading naturally to the picture of a percolating network of bonds, yet non-rigid, subjected to continuous bond breaking and bond forming processes.

For compounds studied by scattering experiments in both the glassy and liquid state, as $ZnCl_2$[6,1] and $GeSe_2$[7,4] the diffraction pattern for the liquid phase show the same features as the low temperature glass including the FSDP, that remain almost unchanged, while the other features show the expected thermal broadening.

A second class of covalent system of current interest is constituted by the amorphous phases of IV group and III-V compound semiconductors, that doesn't show any glass formation process when cooled from their melts at ordinary cooling rates and are currently prepared by various kind of deposition tecniques[8]. The diffraction pattern of the liquid phase near freezing shows clear differences from those of their amorphous state; indeed melting at standard pressure brings elemental and polar III-V semiconductors from tetrahedrally coordinated open structures into metallic liquids having higher density than the solid and first-neighbour coordination number close to seven[9,10]. Their liquid structure is nevertheless quite distinct from that of other liquid metals[11]. Specifically a first-neighbour coordination number of order seven is still relatively low and a second shell of neighbours is seen to lie at a short distance beyond the first shell, in a region of interatomic separations where the pair distribution function g(r) in other liquid metals has

its main minimum. Similarly the liquid structure factor S(k) shows a distinctive shoulder on the large k-side of its main peak, merging into a single asymmetric broad peak with increasing temperature in the liquid phase. The FSDP observed in the amorphous state is no longer evident in the melt. Similar structural feature have been observed in the total diffraction pattern from molten $GaAs$[12].

The similarity in the behaviour of the liquid phase of these elements with that of the previous class lies in the fact that both of them show fluctuations that drive the system towards configuration with local tetrahedral order, due to the tendency of association of atoms in the melt by the formation of covalent bonds. The existence of these kind of fluctuation, with the persistence of some covalent bonding effect in metallic system like liquid Germanium or Silicon was shown by a recent first-principles molecular dynamic simulation made on liquid Silicon[13], by means of the Car-Parrinello method that allows the simultaneous determination of structure and electronic properties. This simulation shows, from the analysis of charge density distributions, that temporary covalent bonds can indeed form in the liquid, the lifetime of the covalent bond being comparable to the characteristic timescale of lattice oscillations. Moreover it was observed that this process of forming and breaking of bonds is characterized by a well defined tendency of density fluctuations towards local tetrahedral order.

A number of theoretical approaches have been presented in the recent literature do deal with the disordered states of the above systems. The basic approach represented by the Car-Parrinello method, combining density functional theory for the valence electrons with molecular dynamics for the ionic cores, has been applied to silicon[13] , $GaAs$[14], and liquid carbon[15]. The metallic melt of elemental semiconductors has also been investigated by the conventional pseudoatom approach of the electron theory of metals[16].

A number of empirical approaches that include three-atom contributions in the potential energy functions in addition to pair potentials has been proposed since the work of Stillinger and Weber on Silicon, (see ref.[17] and references therein) among which we mention that of Vashista on molten and glassy $GeSe_2$ and SiO_2[18], and that of Tersoff on Si and Ge[19]. These model potential are tailored to describe a specific system by fitting their free parameters to properties of a specific phase, by means of MD test runs, and their success depend on a certain extent to the number of properties fitted and on which phase the fit was made.

Even if a more fundamental approach is now available by first principle to deal with the disordered phases of the above system, simple primitive models can be useful to account for common features observed in the above systems. As an example of the value of such models, we quote the work of Iyetomi and Vashista[20], who showed, with the help of a simple model of charged hard spheres, that the presence of a FSDP in chalcogenides glasses arises as effect of medium range correlations due to steric repulsions and local charge neutrality effect. They showed also that the position of this peak cannot be accounted for using pair potential only. Previous explanation of this feature were based on models ol layer-like structures, similar to that present in the crystalline solid, or on the basis of the correlations that arise from the random packing of defined structural units[2].

Model of a certain simplicity that can be relevant to our subject arose in another context, in the statistical mechanical modelling of associated fluids, mainly in the treatment of network-like liquids. Wertheim developed an approch[21] to such associating fluids modelling the elementary units as hard spheres with a fixed number of attraction sites attached on it. The directional interaction is mediated by forces between near-pheripheral sites, that can interact only if the elementary

units have the right relative orientation. This model was investigated mainly by means of Monte Carlo simulations[22]. Another model that has been used in studies of hydrogen bonding in water and methanol is due to Smith and Nezbeda[23], and is similar to Wertheim's scheme, with the variant that the near-peripheral sites acts attracting the center of another units, not another site.

In this thesis we shall present a model able to take into account the peculiar density fluctuations towards local tetrahedral order that characterize the class of materials discussed above and distinguish their behaviour from simple liquid's one. We considered an extension to the melts of III - V and IV group semiconductors of the bond charge model adopted by Phillips[24] to give a picture of the non uniform charge density distribution in crystalline semiconductors and employed by Martin[25] and Weber[26,27] as a simple empirical model to account for the dynamical properties of these materials. A primitive pseudoclassical model for the melt can be constructed by regarding it as a mixture of hard sphere atoms and pointlike bond particles, with mutual attractive interactions which can induce localization of bond particles between pairs of atoms under steric constraints limiting the coordination of an atom by bond particles to a maximum of 4 in tetrahedral configuration. The above model involves only pair potentials between components and thus it can be studied by means of the approximate integral equations of liquid state theory. A particular realization of this model has been examined in relation to liquid germanium, for which very accurate neutron scattering data are available[10]; we shall shown that indeed it gives a semi-quantitative description of liquid germanium's structure near melting, and shows the correct trends of structural features on varying temperature[28]. Equilibrium supercooled states of the model were also investigated in this context, and their structure, as obtained by integral equations techniques, was contrasted with the results of diffraction ex-

periments on amorphous germanium. A considerable effort was devoted to test the accuracy of integral equations techniques for the determination of the pair correlation functions and of structure factors for liquid and supercooled states, by comparison with results obtained in Monte Carlo simulations. Work done on improving the approximations involved in the integral equations approach by the inclusion of Bridge Functions will be also reported here. We shall also present here some empirical melting criteria for III - V semiconductors. The model presented here was also used to study the the freezing of liquid germanium in the framework of the density functional theory of freezing [29].

Chapter 2

Presentation of the Model

2.1 BCM IN THE LATTICE DYNAMICS OF SEMICONDUCTORS

Bond Charge Models are based upon a semiclassical picture of the electron charge density distribution in covalent materials[24,30], and in particular in semiconductors. The electron density distribution in these materials is neither simply the superposition of spherical charge densities centred on the atoms as in purely ionic materials, nor almost uniformly distributed like in simple metals, but a certain amount of charge is accumulated in the covalent bond between adiacent atoms. This can be clearly seen from charge density plots of valence electrons for Ge and for $GaAs$ displayed in fig. 2.1, taken from band structure's calculation of Walter and Cohen[31]. Differential plots in which the charge density of an "isolated" atom at each site is subtracted by the total charge density clearly show that the bond charge is due to chemical bonding and not to simple superposition of individual charge densities[32]. This pileup of charge in bonds is responsible for the "forbidden" reflections observed, for istance, in X- ray scattering experiments on Si[33].

Phillip's idea consist in parting the valence charge density of crystalline semiconductors in two contributions, a spherical charge density located at the atomic

sites, and a point like charge located at the bond, halfway between nearest neighbour atoms in homopolar compounds. A schematic picture of this partition for the charge density is given in fig. 2.2 for an homopolar semiconductor like Si or Ge. Figure 2.3 shows the diamond-type structure of crystalline Germanium after decoration of covalent bonds by bond particles.

As the band structure of Si and Ge is nearly-free-electron like, the bare ion-ion forces are expected to be screened by the charge distribution of valence electrons, and this screening is represented by the diagonal elements of the inverse dielectric matrix $\epsilon^{-1}(\mathbf{q}+\mathbf{G},\mathbf{q}+\mathbf{G}')$. But because of the finite gap between valence and conduction bands, the screening, unlike in metals, is incomplete giving rise to a finite but quite high value for the static dielectric constant ϵ_0 (16 for Ge and 12 for Si), and as a result there remains a residual screened charge of value $+4|e|/\epsilon_0$ at each ion. In order to preserve the charge neutrality, Phillips introduces charges of magnitude $-2|e|/\epsilon_0$ at the bond sites. These bond charges just represent the effect of the off diagonal elements of the inverse dielectric matrix[25,34]. The extension of this picture to III-V semiconductors, in which the bond has a partial ionic character, is straightforward. The partial charge transfer from less to more electronegative atom is reflected in a shift of the bond charge towards the latter, as could be seen in fig. 2.1, and so the equilibrium position of the bond charge in the model should be displaced in such a way to divide the bond lenght in the proportion 5 : 3.

These concepts where exploited by Martin[25] in a study of the lattice dynamics of Silicon. He pointed out that the consideration of the diagonal (metallic-like) part of the screening only leads to pair potentials between silicon atoms, unable to account for the stability of the open tetraedral structure, thus leading to instability against shear modes signaled by imaginary frequencies of TA modes. The

introduction of bond charges constrained to remain at the midpoint of a bond even when atoms are moving, provides through their Coulombic repulsion a bond-bending force and so gives rise to an effective non central interaction between ions which stabilizes the structure. Martin found an overall satisfactory agreement with the experimental phonon dispersion curves, being able to reproduce at least partially the characteristic flattening of TA modes along the [100] and [111] directions in the Brillouin zone, and values of elastic constants. He also used a simple two parameter model to account for the main features of the dispersion relations, allowing Coulomb interaction between ion-ion, ion-BC and BC-BC and introducing a short range force between nearest-neigbour ions only, to account for the deviation from the Coulomb force due to the diagonal screening, which reaches the asymptotic value for distancies of the order of the atomic spacing.

These ideas where developed by Weber who proposed a simple empirical model with few parameters, the Adiabatic Bond Charge Model, that well describes the lattice dynamics of group IV elements[26] (C- diamond, Ge, Si, $\alpha - Tin$) and III-V semiconductors[27], and has the same importance for the lattice dynamics of semiconductors as the shell model[35] for the lattice dynamics of ionic systems.
Weber removed the constraint that B. C. should follow the atomic motion istantaneously, allowing them to move adiabatically like the electronic shells in the shell model, by providing an appropriate ion-B.C. force to fix their equilibrium position at the midpoint of the bond. The four kind of interactions allowed in the model are, as sketched in in fig. 2.4:

- Coulomb forces betweeen charges, with coupling parameter $\gamma_{ij} = Z_i Z_j / \epsilon_0$.
- Short range forces betweeen nearest-neighbours
  (a) ion - ion central interaction
  (b) ion - B. C. central interaction

(c) B. C. - B. C. non-central interaction

As we have already seen, forces of type (a) accounts for the effects of diagonal screening in semiconductors, while interactions of type (b) and (c) are characteristic of the covalent bond, representing respectively the strenght of the bond and the interaction between neighbouring bonds, due to variation in the s-p ibridization when the angle between bonds changes. There are only 4 parameters, related to the couplings of the different interactions involved, that could be fitted matching an equal number of relations. These are derived requiring that the observed frequencies are reproduced at some high simmetry points in the Brillouin zone. In the extension to III-V semiconductors 6 parameters are necessary, being present now one interaction of type (b) and (c) for each type of ion (the charges of the two ions are set equal, so still one parameter is necessary for Coulomb coupling). The good agreement with the observed dispersion relations and elastic costants obtained by the model is shown in fig. 2.5 for the case of Ge.

Weber examined also the importance of the Coulomb interaction in his model, considering the case in which they are dropped by setting $\gamma = 0$, and found that the overall agreement remains good, meaning that their effect is marginal. The dispersion relations of this uncharged model are compared in fig. 2.6 to that of the full model, already shown in fig. 2.5. He showed also that the characteristic flattening of TA modes depends on the relative importance of the ion-bc and bc-bc coupling. When the former is weaker than the latter, atoms vibrate in a rigid lattice of bond charges as almost decoupled oscillators with small force constant, and only in the long wavelenght limit, when atoms and b.c. move in phase, the rigidity is trasferred also to the atomic motion. The variation of this ratio can thus account for the trend in TA mode flattening, which is more pronounced in less covalent systems as $\alpha - Tin$, decreases going from Ge to Si and is not present

in diamond. The success of this models is mainly due to the introduction of only few interaction of short range type with a clear physical interpretation.

In a recent study, Fleszar and Resta[36] have shown that the BCM gives also correct values of the real space force constants, and of the interplanar force constants as compared with the results of first- principles calculations, and that the presence of BC with their interactions accounts for an effective atom-atom coupling up to the 13th neighbour.

The adiabatic bond charge model found recent application to the lattice dynamics of polar semiconductor superlattices[37], of the polymorphic phases of Si and Ge[38], to the study of the surface phonons of the reconstructed $Si(111)$ 2×1 and of the $Si(111) + H$ 1×1 surfaces[39]. It was also applied for examining molecular vibration in diatomic and polyatomic molecules[40], a field in which Valence-Force- Fields models have found prevalent applications. Concepts relaying on the BCM, either in the Phillips-Martin version or in the Weber version, were applied also to the non-linear optical properties of covalent AB compounds[41], and to the infrared absorption and Raman spectra of group-IV elements[42].

2.2 BCM FOR SEMICONDUCTOR MELTS

As we have seen in the preceding section, the success of the BCM in reproducing the lattice dynamics of semiconductors relies upon the simple physical representation that it gives of the forces due to the covalent bond, namely the introduction of bond charges as centres of forces to account for the directional interactions between atoms, involved in chemical bonding. We want to extend this simple picture to treat interatomic forces in the melts of IV group and III - V semiconductors. The underling physical assumption for this extension is that, even if these systems

show metal-like conductivity[43] in the molten state, the formation and breaking of covalent bonds in the melt play still an important role, driving the system towards density fluctuation of local tetrahedral order. It was shown by a recent first-principle simulation on molten Silicon by the Car-Parrinello method[13] that this is indeed the case.

In the spirit of BCM we examined a primitive model for the melt regarding it as a mixture of atoms and Bond Particles, in which the atom-atom interaction is represented at the most elementary level by hard sphere repulsion, and an appropriate ion-BP interaction provides a stable equilibrium position for the Bond Particles, which are now free to leave the bond. This attractive interaction can induce localization of bond particles between pair of atoms, constituting a "bond" between them; the directionality in the interaction between atoms is accounted for by the steric restriction that at most 4 BP can localize in tetrahedral configuration around one atom. The main aim in examining the model as formulated above is to follow the structural evolution of both the atomic and BP component as the temperature is lowered from hot liquid states to strongly supercooled states. Directionality of effective atom-atom interaction and angular interatomic correlations are progressively built into the model as localization of BP sets in and grows. In the liquid state this amounts in the presence of a fluctuating network of bonds, with the occurence of fluctuations that lead to the temporary formation of tetrahedral open units of four atoms "bonded" to a central one. One could follow the increasing correlation between such units on lowering the temperature, ending eventually in the formation of a permanent network with stable bonds.

A Model for Liquid Germanium

We consider a two-component fluid of hard spheres, with component A (Ge atoms) and B (Bond Particles) having number density n_A and $n_B = 2n_A$ at temperature T. The hard-sphere interactions are characterized by three distances of closest approach (σ_{AA}, σ_{AB} and σ_{BB}, say). In the problem at hand the relevant values of the hard-sphere contact distances are asked to satisfy the approximate relations

$$\sigma_{AA} \simeq 2\sigma_{AB} \leq \mathrm{d} \qquad\qquad \sigma_{BB} \sim \sqrt{\frac{2}{3}}\,\mathrm{d} \tag{2.1}$$

where d represents the bond-lenght. These relations imply that, even though the B component is essentially point-like compared with the A component, no more than four B particles can be found in immediate contact with any A particle. This feature of the model (non-additivity in excluded volume effect) is to be contrasted with the primitive model of a liquid alloy as a mixture of hard spheres[44,45], in which additivity of hard-spheres diameters is imposed by setting $\sigma_{AB} = (\sigma_{AA} + \sigma_{BB})/2$.

We next introduce interactions which lead to strong relative ordering of the two components in the liquid, considering two alternative cases. The first choice (Localized Attraction Model- LAM) is similar in spirit to the Weber BCM and introduces an attractive interaction between A and B particles in the form of a narrow potential well centred at the distance d/2 from the centre of each A particle and uniformely spread over its surface (see fig. 2.7). The well is taken to have a gaussian shape of half-width σ and depth V, with $\sigma \simeq \mathrm{d}/2 - \sigma_{AB}$ is chosen narrow so that there is a well defined bond- lenght d. We may explicitly note here that the role played in Weber's model by bond bending non-central forces between Bond Particles is taken up in our model for the liquid, at appreciable values of the

A-B coupling strenght, by the simple requirement made on the distances of closest approach between them.

The well depth enters the model only in units of the thermal energy k_BT, yielding a coupling strenght parameter $V^* = V/k_BT$ which will be allowed to increase continuously from zero in order to follow the process of localization of bond particles. For liquid germanium near freezing, estimating V from the valence-conduction band gap of the crystal ($V \simeq 0.7eV$), we anticipate $V^* = 6$.

The second alternative that we had explored[28] for the origin of relative order of the components of the liquid is closer to Phillips' original BCM. The hard-spheres are assigned charges in amounts Z_Ae and Z_Be respectively, with $Z_B = 1/2Z_A$.

The A-B coupling strenght is now measured by the 'plasma parameter' $\Gamma = Z_B^2e^2/(ak_BT)$, the lenght a being related to the liquid density by $a = (4\pi n_A)^{-1/3}$. Again this parameter will be allowed to increase continuously from zero. Phillips' original estimate was $|Z_B| \simeq 0.5$ corresponding to two electronic charges screened by the dielectric constant of the material, while fits in the BCM of Martin and Weber gives respectively values of 0.65 and 0.40. The corresponding value for Γ appropriate to Germanium near freezing is in the range 50-20.

A combination of short range attraction and Coulomb forces could also be possible, but relying on Weber analysis of his model, we think that also in the liquid near freezing only short range forces are determinant for structural features.

The calculations reported in Chap. 4 refer to two choices of the liquid density taken from experiments. As we expect the average bond-lenght to be different in the melt from the value found in the amorphous solid, and as the narrow well considered by us doesn't allow the bond lenght d to vary on temperature, we chose

also two different values for d, read by the $Ge - Ge$ first- neighbour distance in neutron scattering experiments.

For liquid Germanium at $T = 1253\ K$, which is above the freezing point at atmospheric pressure (1210 K), one has $n_A = 0.0461 \mathring{A}^{-3}$ from rif. [43] and d $= 2.63 \mathring{A}$ from the neutron diffraction experiment of Gabathuler and Steeb[46]. In amorphous Germanium, on the other hand, the density depends on the film deposition rate and on film thickness, being at most equal to 97% of the crystalline density (see for istance ref. [47]). We have considered such a value of density as our second choice, in combination with the value d $= 2.46 \mathring{A}$ from the diffraction experiment of Etherington *et al.*[48] on amorphous Germanium at room temperature. This value of the bond-lenght is pratically the same as in crystalline germanium. Finally the various choices that we shall illustrate for the hard spheres contact distances and the well half-width, are collected for convenience in table 2.1. We shall comment later on these specific choices as the opportunity arises.

TABLE 2.1 Sets of model parameters used in the calculations

	$n_A(\mathring{A}^{-3})$	d (Å)	σ_{AA}/d	σ_{AB}/d	σ_{BB}/d	σ/d
Set 1	0.0461	2.63	0.94	0.475	0.80	0.050
Set 2	0.0429	2.46	0.95	0.475	0.76	0.050
Set 3	0.0429	2.46	0.98	0.475	0.81	0.050
Set 4	0.0429	2.46	0.98	0.500	0.81	—

Extension to III - V Semiconductors

Let us consider here as an example a straightforward extension of the LAM model to the description of III-V semiconductors. We shall adopt now a three component fluid composed by two kind of atoms, A1 and A2, and one kind bond particles B, so that six close contact distances $\sigma_{\alpha\beta}$ have to be chosen. In the case of Germanium only one of this distances, namely σ_{AA}, is an indipendent parameter, and has been slightly adjusted in our calculations to give agreement with the height of the first peak in S(k) in diffraction experiments, while σ_{BB} and σ_{AB} were fixed by the relation (2.1). In III-V compounds the BP divides the bond lenght d in two parts d_{A1}, d_{A2} with $d_{A1}/d_{A2} = 3/5$, is the ratio between the number of valence electron in each atom. It should be noticed that the equilibrium position of BP is given by the location of the minimum in the A-B well, while σ_{AB} essentially represents the repulsive part of the A-B potential. The distances $\sigma_{B\alpha}$, (α = A1 or A2) should satisfy the approximate relation $\sigma_{B\alpha} \leq \mathrm{d}_{\alpha}$. Now σ_{BB} is fixed by the request of tetrahedral coordination of BP around A1 leading to

$$\sigma_{BB} \sim \sqrt{\frac{2}{3}}\, \mathrm{d}_{A1} < \sqrt{\frac{2}{3}}\, \mathrm{d}_{A2} \tag{2.2}$$

The tetrahedral coordination around each atom is still satisfied, but (2.1) shows that it is more strictly enforced on atoms of type A1, reflecting the different rigidity against bond bending on atoms of different kinds. A more quantitative treatment of this effect requires the adoption of continuous repulsive potential for BB interaction, whose stepness is related to the different rigidity on bond bending on each atom.

The atomic diameters $\sigma_{\alpha\alpha}$ can be chosen close to the actual sizes of the two kind of atoms, and the distance of close contact between different atomic species σ_{A1A2}

can be fixed by the request of additivity of the atomic diameters; this choice gives only two parameters to be slightly fitted.

Consideration of non-additive hard sphere diameters between atomic components has been useful in describing the different excluded volume effects in the interactions between like and unlike atoms due to chemical bonding effects in models for $Ni-Y$[49] and $Ni-Ti$ [50] metallic glasses, or to enforce fourfold coordination in a model for liquid $ZnCl_2$[51], but is not necessary here, as the chemical bonding is accounted for by the presence of BP. The non additivity of the interactions is considered only, as we have seen, for the interactions A-BP BP-BP A-A.

Notice that now the relation $\sigma_{\alpha\alpha} \leq \mathrm{d}_\alpha$ where (α =A1 or A2) may be violated, meaning bond particles localized not at the surface but well inside one of the atomic spheres.

Two BP-atom attractions are now needed to account for covalent bonds between A1 and A2 atoms, i.e. one for A1-BP the other for A2-BP, and the same gaussian well can be used, centred at d_{A1} for A1 atoms and at d_{A2} for A2 atoms, with the depth fixed again from the value of the gap.

As there is evidence that a small amount of wrong-bonds between like elements may occur both in the liquid and amorphous state[14], it might be necessary to introduce two other different wells of suitable depth to account for A1-A1 and A2-A2 bonding, and their influence on the structure might sistematically be studied. This kind of bonding should certainly be accounted for in studies of $Si-Ge$ systems, or other mixtures of IV group elements. Maybe the case that for such systems the equilibrium position for BP in unlike bonds should also be shifted toward the most electronegative atom.

Another point that can be explored by this model is whether the partial ionicity of these compounds is completely accounted for in this scheme by the shift in the

equilibrium position of the BP in an uncharged system, or it should be necessary to place ionic charges of different sign on atoms of different kind. One can thus study to what extent this choice influences the structural properties.

2.3 MELTING CRITERIA

As we shall show in Chap. 4, the liquid structure for the models considered here shows the same qualitative structure of liquid Ge when values of the coupling strenght parameters assume approximatively values of $V^* \simeq 7.5$ for the LAM and $\Gamma \simeq 24$in the other BCM. We notice that these values are close to those anticipated in Sec. 2.1 from the observed band-gap E_g in the crystal and from the extimated value of -2 for the bare bond charge, in the Phillip's scheme, that leads to a coupling $4/\epsilon_0$ betwen them.

We now ask whether there is any generality to these results. Namely, we ask whether for semiconductors which melts with a break-up of chemical bonding, one can formulate empirical melting criteria in the forms

$$\frac{E_g}{k_B T_m} \simeq constant \tag{2.3}$$

or

$$\frac{4e^2}{\epsilon_0 a k_B T_m} \simeq constant \tag{2.4}$$

at the melting temperature T_m. First we looked for linear correlations between T_m and E_g or T_m and $n^{1/3}/\epsilon_0$ where n is the number of atoms per unit volume.

Figure 2.8 shows that there is an approximate linear relation in both cases. Data for T_m, E_g, ϵ_0 used in the figure are taken from *Landolt-Börnstein* tables [52]. The constant of proportionality are found to be approximately equal to 10 for

(2.3) and 20 for (2.4), that are essentially in agreement with the values obtained in our model. We note also that criteria (2.4) is well satisfied, being almost all the values on the same line, and this line has intercept zero. In the other case the values are more scattered around a line, and the value for $E_g = 0$ lays at $T_m \simeq 740K$; being the value $740/k_BT$ of order unity at the melting temperature involved, we can still say that the criteria (2.3) is approximatively satisfied.

The melting criteria involving the bandgap was not unexpected, and a melting criterion relating the melting temperature to the band gap was already proposed by Godefroy and Aigrain[53]. The melting criterion based on the bond charge concept is less obvious and its empirical verification give additional support to the qualitative usefulness of Phillip's ideas.

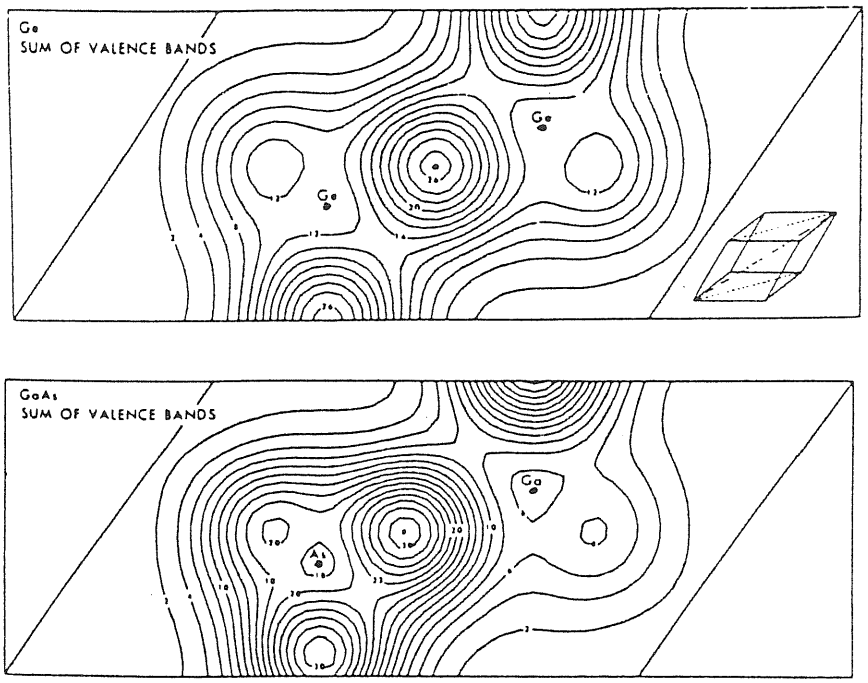

Fig. 2.1 – Total valence electron charge density (in units of electronic charge, e) in the (1 -1 0) plane, for crystalline Germanium (upper figure) and Gallium Arsenide (lower figure). The insert shows the direction of the plane in the unit cell. From Walter and Cohen, ref.[ ].

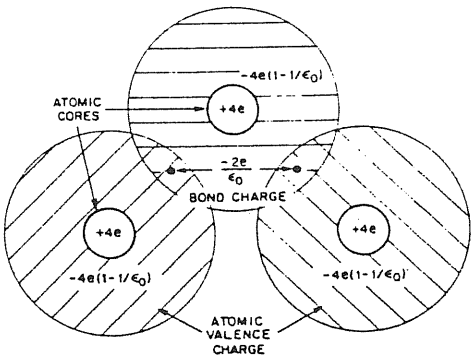

Fig. 2.2 – Separation of valence charge distribution in diamond- type semiconductors into atomic and bonding parts. From Phillips, ref.[b].

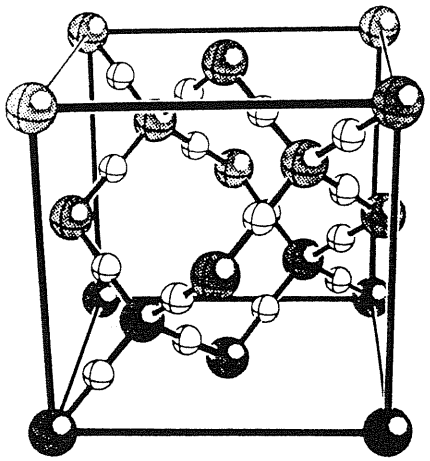

Fig. 2.3 – Cubic cell of crystalline Germanium showing decoration of interatomic bonds by bond particles. In crystallography this decorated structure is know as the ideal β-crystobalite structure for SiO_2.

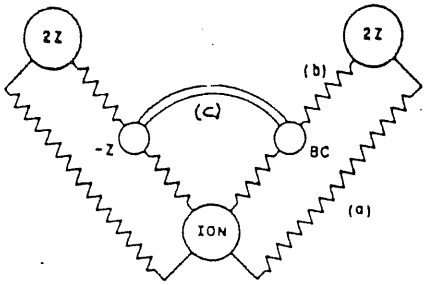

Fig. 2.4 – Schematic presentation of the short range interactions used in the Adiabatic Bond Charge Model of Weber: (a) ion-ion (central); (b) ion-BC (central); (c) BC-BC (non-central). From Weber refs.[,].

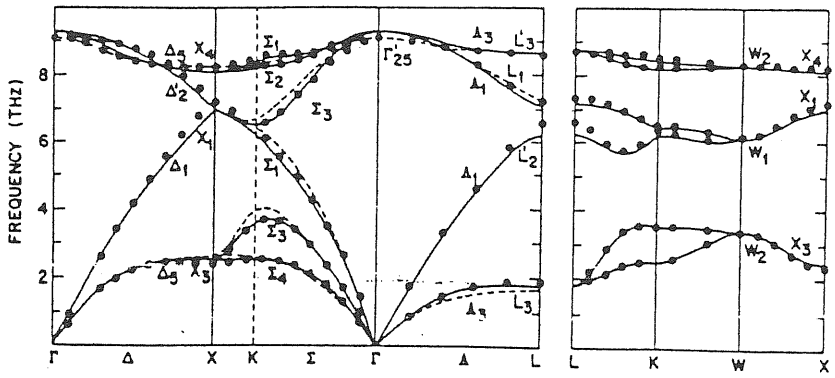

Fig. 2.5 – Phonon dispersion curves for Germanium. Solid lines show the results of Weber's Adiabatic Bond Charge Model compared with experimental values (points). From Weber ref.[ ].

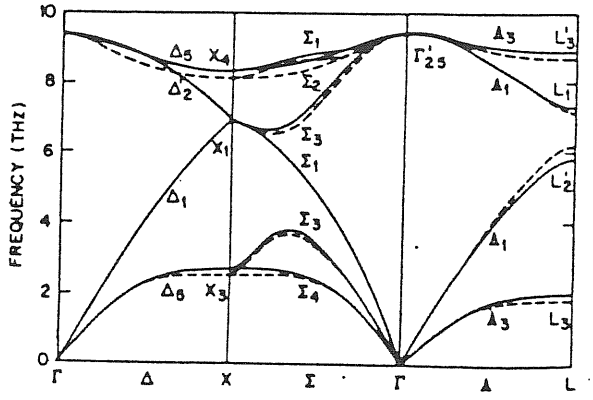

Fig. 2.6 – Phonon dispersion curves for Germanium as calculated from Weber's BCM with short-range forces only (solid lines) in comparison with the results showed in fig.2.4 for the full model (dashed lines). From Weber ref.[ ].

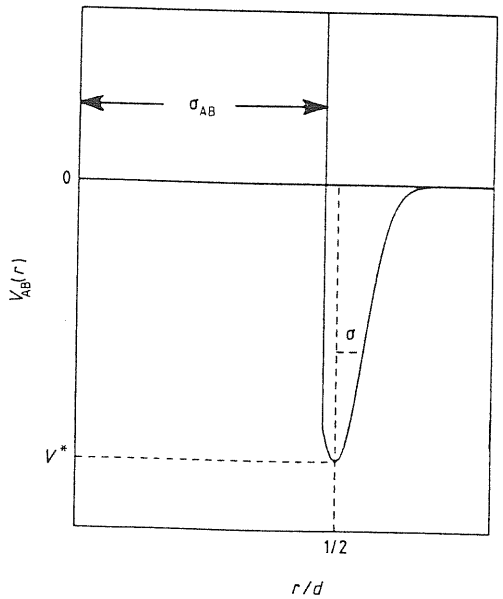

Fig. 2.7 – Atom-Bond Particle interaction potential in the LAM.

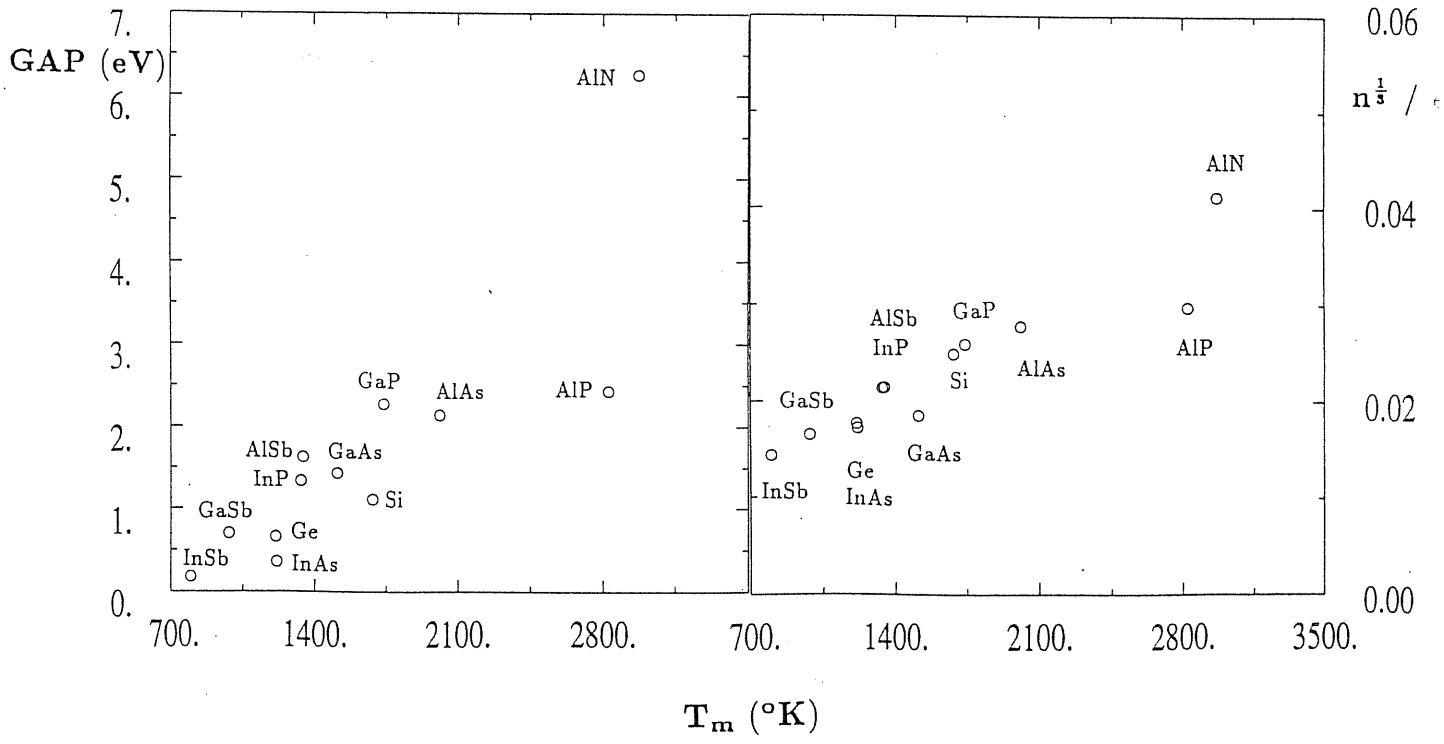

Fig. 2.8 – Correlation of the melting temperature T_m of elemental semiconductors and III-V compounds with the valence-conduction band gap E_g (left) and with the quantity $n^{1/3}/\epsilon_0$ (right), where n is the number of atoms per unit volume and ϵ_0 the static dielectric constant of the crystal.

Chapter 3

Methods for the Study of the Model

We present here a summary of concepts from the theory of liquids, including the definitions of the relevant structural quantities (i.e. pair correlation functions and structure factors), and a description of the statistical mechanical methods we employed in the study of our model, namely integral equations and Monte Carlo simulations.

In order to make the presentation of results in the following chapters as simple as possible, we include here for later reference all the technical details about numerical calculations. A general reference for this chapter is the book by Hansen and McDonald[54].

3.1 DEFINITIONS

Notations for Fourier Transforms

We shall adopt the following notation to indicate a 3D-Fourier transform of a function of a vector

$$\tilde{f}(\mathbf{k}) = \int f(\mathbf{r})\ e^{-i\ \mathbf{k}\cdot\mathbf{r}}\ \mathrm{d}\mathbf{r} \qquad (3.1a)$$

If f depends only on the modulus of $\mathbf{r}$, one can write the integral in polar coordi-

nates as

$$\tilde{f}(k) = \int_0^{2\pi} \mathrm{d}\phi \int_0^{\infty} \mathrm{d}r \int_{-1}^{1} \mathrm{d}\cos\theta \; r^2 f(r) \; e^{-ikr\cos\theta} = \\ = \frac{4\pi}{k} \int_0^{\infty} r f(r) \sin kr \; \mathrm{d}r \tag{3.1b}$$

In the same way we can express the inverse fourier transform

$$f(\mathbf{r}) = \frac{1}{(2\pi)^3} \int \tilde{f}(\mathbf{k}) \; e^{i\,\mathbf{k}\cdot\mathbf{r}} \; \mathrm{d}\mathbf{k} \tag{3.2a}$$

when f depends only on the modulus of $\mathbf{k}$

$$f(r) = \frac{1}{2\pi^2 r} \int_0^{\infty} k\tilde{f}(k) \sin kr \; \mathrm{d}k \tag{3.2b}$$

Number Density

In what follows we shall always denote with n the **number density** of an homogeneous system, that is the number of atoms per unit volume measured in $\mathring{A}^{-3}$. On the contrary the mass density, i.e. mass per unit volume will be denoted with ρ. Dealing with m-component systems, n is the **total** number density, while n_α ($\alpha = 1, 2, ..., m$) are the **partial** number densities, and $x_\alpha = n_\alpha/n$ are the molar fractions or relative concentrations for the component of type α.

Pair correlation Functions and structure Factors

At present the only structural quantities directly measurable by experiment for disordered homogeneous systems like a liquid, a glass or an amorphous solid are the pair static correlation function (or radial distribution function) $g(r)$ and the static structure factor $S(k)$. They are related in the former system to the average (time average) equilibrium local fluctuations of density, and to the correlation between the position of particles, averaged over the sample, in the latter. These functions give some information about the spatial correlations of pair of particles in the range of few (from 0 to 10-12) Ångstrom.

In a X-ray scattering experiment, and in a neutron scattering experiment under certain conditions, the coherent scattered intensity at a given angle is proportional to $S(k)$, k being the trasferred momentum in the scattering process. In Statistical Mechanics the structure factor describes the correlation between density fluctuation of wavelenght $\lambda = \frac{2\pi}{k}$ in two different points at equal time

$$S(\mathbf{k}) = \frac{1}{N} \left\langle \sum_{i=1}^{N} \sum_{j=1}^{N} e^{i\ \mathbf{k} \cdot (\mathbf{r}_i - \mathbf{r}_j)} \right\rangle$$

where the brackets indicate a statistical average over a canonical ensemble of N particles.

The pair correlation function for an homogeneous system can be defined as the probability distribution function for finding any particle around any other particle at a distance r. It describes at a pair level the average local arrangement of atoms in the system. It's useful to introduce another function, called also pair correlation function or total correlation function $h(r) = g(r) - 1$, describing the spatial deviation from the uniform mean density.

The link between the pair correlationfunction and the density-density autocorrelation function at equal time $G(r, t = 0)$, describing spatial density fluctuation is given by

$$G(\mathbf{r}, t) = \frac{1}{N} \left\langle \sum_{i=1}^{N} \sum_{j=1}^{N} \int \delta[\mathbf{r}' + \mathbf{r} - \mathbf{r}_i(t)]\ \delta[\mathbf{r} - \mathbf{r}_j(0)]\ \mathrm{d}\mathbf{r}' \right\rangle \tag{3.3}$$

$$G(\mathbf{r}, 0) = ng(\mathbf{r}) + \delta(\mathbf{r})$$

The structure factor is related to the pair correlation function by a fourier transform, giving for $\mathbf{k} \neq 0$ the relation

$$S(\mathbf{k}) = 1 + n\tilde{h}(\mathbf{k}) \tag{3.4}$$

Dealing with multi-component systems we need more than one pair distribution function to describe its structure; for two component fluids with particles

of type A and B, three functions g_{AA}, g_{AB} and g_{BB} are required. The partial distribution function $g_{\alpha\beta}(r)$ represents the probability distribution for finding any particle of type α (α = A or B) at a distance r around any particle of type β (β = A or B) , so that $4\pi r^2 n_\beta g_{\alpha\beta}(r)$ represents the average number of particle of type α within a spherical shell of radius r centred around one particle of type β.

The cumulative coordination numbers $N_{\alpha\beta}(R)$ are evaluated from the integral

$$N_{\alpha\beta}(R) = 4\pi n_\beta \int_0^R r^2 g_{\alpha\beta}(r)\ \mathrm{d}r \tag{3.5}$$

Notice that $g_{\alpha\beta} = g_{\beta\alpha}$ but $N_{\alpha\beta} \neq N_{\beta\alpha}$ if $n_\alpha \neq n_\beta$.
The near-neighbour coordination numbers that we shall report are obtained setting the integration limit R equal to the position of the first minimum in the corresponding $g_{\alpha\beta}(r)$.

The partial structure factors can be defined in several ways[11]; among various definition we chose that due to Ashcroft and Langreth[44]

$$S_{\alpha\beta}(k) = \delta_{\alpha\beta} + \sqrt{n_\alpha n_\beta}\ \ \tilde{h}_{\alpha\beta}(k) \tag{3.6}$$

which has, for like particles, the same form as eq. (3.4) for the one component system.

Direct correlation Function and the Ornstein-Zernicke relation

For the theoretical description of liquids it's useful to introduce another kind of correlation function.
The excess Helmoltz free energy of an inhomogeneous system can be expressed as a functional $F_{ex}[n(\mathbf{r})]$ of the one particle density $n(\mathbf{r})$, which is the probability density of finding any particle at the position $\mathbf{r}$. We can define the n-particle direct correlation function taking the functional derivatives

$$c^{(n)}(\mathbf{r}_1, ..., \mathbf{r}_n) = \left.\frac{\delta^n F_{ex}}{\delta n(\mathbf{r}_1), ..., \delta n(\mathbf{r}_n)}\right|_{n(\mathbf{r}_i)=n} \tag{3.7}$$

around the homogeneous state.

For an homogeneous system $c^{(n)}$ depends only on the distance between particles $r_{ij} = |\mathbf{r}_i - \mathbf{r}_j|$, and so

$$c^{(2)}(\mathbf{r}_1, \mathbf{r}_2) = c^{(2)}(r)$$

$$c^{(3)}(\mathbf{r}_1, \mathbf{r}_2, \mathbf{r}_3) = c^{(3)}(r_{12}, r_{23}, r_{13})$$

Direct correlation functions are related to the total correlation functions through the Ornstein-Zernicke (O.Z) relation

$$h(r) = c(r) + n \int c(|\mathbf{r}' - \mathbf{r}|)h(r')\ \mathrm{d}\mathbf{r}' \tag{3.8a}$$

that can be written using fourier transform as

$$\begin{aligned} \tilde{h}(k) &= \tilde{c}(k) + n\tilde{c}(k)\tilde{h}(k) \\ \tilde{h}(k) &= \frac{\tilde{c}(k)}{1 - n\tilde{c}(k)} \end{aligned} \tag{3.8b}$$

Using eqs. (3.8b) and (3.4) one can find the following relation between c(k) and S(k)

$$S(k) = \frac{1}{1 - n\tilde{c}(k)} \tag{3.9}$$

The generalization of the O.Z. integral equation to a two component system leads to the Pearson-Rushbrooke integral equations

$$h_{\alpha\beta}(r) = c_{\alpha\beta}(r) + \sum_{\delta} n_\gamma \int c_{\alpha\delta}(|\mathbf{r}' - \mathbf{r}|)h_{\delta\beta}(r')\ \mathrm{d}\mathbf{r}' \tag{3.10a}$$

$$\tilde{h}_{\alpha\beta}(k) = \tilde{c}_{\alpha\beta}(k) + \sum_{\delta} n_\gamma \tilde{c}_{\alpha\delta}(k)\tilde{h}_{\delta\beta}(k) \tag{3.10b}$$

where the sum runs over the two components of the system. A relation between $S_{\alpha\beta}$ and $c_{\alpha\beta}$ similar to eq. (3.9) is easily written in matrix form as

$$\Big(S_{\alpha\beta}(k)\Big) = \Big(\delta_{\alpha\beta} - \sqrt{n_\alpha n_\beta}\ \ \tilde{c}_{\alpha\beta}(k)\Big)^{-1} \tag{3.11}$$

3.2 INTEGRAL EQUATIONS

Integral equation theories of liquids provide a way for determining the structure, at the level of pair correlation, and the thermodynamic properties of equilibrium states for fluids whose particles interact with pair potentials only. In the simplest version we shall sketch here, the theory apply to model fluids composed by "simple" particles, regarded as isotropic, structureless objects (i.e. "atomic" or "ionic" liquids), but generalizations also exists to deal with molecular[54] and associated fluids[21].

For studing our model we are interested in the case of a two component system of particles interacting with pair potentials only, that is a system whose potential energy V is factorizable as a sum of pair interaction $v_{\alpha\beta}(r_{ij})$.
We have two sets of equations connecting the unknown functions $g_{\alpha\beta}$ and $c_{\alpha\beta}$ with the pair interaction $v_{\alpha\beta}$.

– one is the set of integral equations (3.10), which generalize the O.Z. equation relating $c_{\alpha\beta}$ and $h_{\alpha\beta}$

– the other is an exact relation, called closure relation

$$g_{\alpha\beta}(r) = e^{-\Phi_{\alpha\beta}(r) + h_{\alpha\beta}(r) - c_{\alpha\beta}(r) - B_{\alpha\beta}(r)} \tag{3.12}$$

where $\Phi_{\alpha\beta}(r) = \beta c_{\alpha\beta}(r)$ is the pair potential in units of temperature. This relation has originally been derived by diagrammatic methods[55] (see also ref.[56]) , from the formal series expansions of g and c in powers of the density, but it can be derived also by means of a density functional formalism[57][58][59]. The functions $B_{\alpha\beta}(r)$ in the diagrammatic derivation are expressed as the sum of the so called "elementary diagrams" or "bridge diagrams", which have a precise topological characterization (see ref.[54]); on the other hand also in density functional

derivation the bridge function can be expressed by a series

$$B_{\alpha\beta}(r) = \sum_{\nu=4}^{\infty} B_{\alpha\beta}^{(\nu)}(r) \tag{3.13}$$

For a one-component system, the generic term in this sum takes the expression

$$B^{(\nu)}(r) = B^{(k+2)}(r) = -\frac{n^k}{k!} \int c^{(k+1)}(\mathbf{r}, \mathbf{r_1}...\mathbf{r_k}) h(\mathbf{r_1})...h(\mathbf{r_k})\ \mathbf{dr_1}...\mathbf{dr_k} \tag{3.14}$$

the first term of the series being

$$B^{(4)}(r) = -\frac{n^2}{2} \int c^{(3)}(\mathbf{r}, \mathbf{r_1}, \mathbf{r_2}) h(\mathbf{r_1}) h(\mathbf{r_2})\ \mathbf{dr_1 dr_2} \tag{3.15}$$

We shall deal extensively with the bridge functions in a later section.

The two sets of equations (3.10) and (3.12) constitute a closed set of three coupled nonlinear integral equations, usually expressed in the unknown function $\gamma_{\alpha\beta}(r) = h_{\alpha\beta}(r) - c_{\alpha\beta}(r)$, that can be solved from the knowledge of the potential $\Phi_{\alpha\beta}(r)$, provided that we have chosen a suitable analitical expression or an approximation for the bridge functions. The advantage in casting the equations in terms of $\gamma_{\alpha\beta}(r)$ is that this function is smooth even for discontinuous potentials, like the hard-sphere one, while both $g_{\alpha\beta}(r)$ and $c_{\alpha\beta}(r)$ are discontinuous at the points of discontinuity in the potential (see ref.[54]).

Different kind of approximate integral equations can be obtained assigning to $B_{\alpha\beta}(r)$ a specific functional form in terms of $\gamma_{\alpha\beta}(r)$. We present here a list of approximate closure relations that are relevant for our work, classifying them from the functional form that they show for the bridge functions.

HNC EQUATIONS – the simplest choice for the bridge functions, i.e. neglecting completely the contribution of the elementary diagrams, by setting $B_{\alpha\beta}(r) = 0$, gives rise to the Hyper-Netted-Chains equations

$$g_{\alpha\beta}(r) = e^{\,-\,\Phi_{\alpha\beta}(r) + h_{\alpha\beta}(r) - c_{\alpha\beta}(r)} \tag{3.16}$$

It is superior to other closures in the treatment of charged systems, where it is accurate for a wide range of parameters, as this approximation maintains some sum rules, involving correlation functions, that ensure the overall charge neutrality of the system[60] (for extensive refs. on this closure see the review article of Ichimaru[59]).

MSA APPROXIMATION – The Mean Spherical Approximation deals with system of hard-spheres plus a potential tail and correspond to the choice

$$B_{\alpha\beta}(r) = \begin{cases} -\ln\left(h_{\alpha\beta}(r)+1\right) + h_{\alpha\beta}(r) & if \quad r > \sigma_{\alpha\beta}(r) \\ +\infty & otherwise. \end{cases} \tag{3.17a}$$

that substituted in (3.12) gives a more familiar relation

$$\begin{cases} g_{\alpha\beta}(r) = 0 & if \quad r < \sigma_{\alpha\beta}(r); \\ \Phi_{\alpha\beta}(r) = -c_{\alpha\beta}(r) & otherwise. \end{cases} \tag{3.17b}$$

that is motivated on the physical ground by the requirement of excluded volume effect and correct asymptotic behaviour of $c_{\alpha\beta}(r)$. It also found extensive applications as in many cases can be solved analitically. It can be generalized to soft repulsive potentials plus an attractive part (Soft MSA)

PY EQUATIONS – The Percus-Yevick closure (PY) corresponds to the choice

$$B_{\alpha\beta}(r) = \gamma_{\alpha\beta}(r) - ln[1+\gamma_{\alpha\beta}(r)] \tag{3.18a}$$

that when substituted into eq. (3.12) gives

$$g_{\alpha\beta}(r) = [1+\gamma_{\alpha\beta}(r)]e^{-\Phi_{\alpha\beta}(r)} \tag{3.18b}$$

or alternatively

$$c_{\alpha\beta}(r) = g_{\alpha\beta}(r)\left(1 - e^{\Phi_{\alpha\beta}(r)}\right) \tag{3.18c}$$

It was derived by diagrammatic methods by neglecting a particular class of bridge diagrams, and resumming the remainder. It is superior to other closures in the

case of hard spheres, for which it reduces to the MSA, and it is analitically solvable for one-component hard-sphere and two component additive hard-spheres systems. As the $g_{\alpha\beta}(r)$ is not positive definite in this approximation, it can show for attractive potentials at strong coupling strenght negative values at the position of deep minima.

As a consequence of the approximations made on the bridge functions, one obtains an approximate theory for the structure that can be still accurate over a wide range of parameters for a certain class of systems, but one as to check the limits of validity of the chosen approximations contrasting its predictions with "exact" results provided by computer simulation. The exploration of the accuracy of various approximate closure in the case of the LAM in one of ther main arguments treated in this thesis.

Another consequence of the approximation is a certain amount of thermodynamic inconsistency, as a consequence of the violation of certain sum rules between correlation functions. This means that some thermodynamic quantities can have different values if one computes them through different routes. The amount of thermodynamic consistency can be used to judge the goodness of the approximation.

EMPIRICALLY MIXED INTEGRAL EQUATIONS

The empirical observations that HNC solution and PY solution bracket the exact solution as it emerges from simulations, gave rise to the Roger-Young mixed closure[61], that interpolates between the PY closure at short distances and the HNC one at long range. As a statement on the bridge functions, it can be expressed by

$$B_{\alpha\beta}(r) = \gamma_{\alpha\beta}(r) - \ln\left[1 + \frac{e^{f_{\alpha\beta}(r)\gamma_{\alpha\beta}(r)} - 1}{f_{\alpha\beta}(r)}\right] \qquad (3.19a)$$

that gives the closure relation

$$g_{\alpha\beta}(r) = e^{-\Phi_{\alpha\beta}(r)}\left[1 + \frac{e^{f_{\alpha\beta}(r)\gamma_{\alpha\beta}(r)} - 1}{f_{\alpha\beta}(r)}\right] \tag{3.19b}$$

where f represents a mixing function of the form $f_{\alpha\beta}(r) = 1 - e^{-r/\xi_{\alpha\beta}}$ and $\xi_{\alpha\beta}$ are parameters that can be fixed by the requirement of Thermodynamic Consistency (TC) of the theory. In the same spirit another mixed closure have been proposed by Hansen and Zerah [62]; it interpolates between the HNC closure at long range, and the Soft-MSA approximation (a generalization of the MSA closure)at short range. It is expressed by

$$B_{\alpha\beta}(r) = \gamma_{\alpha\beta}(r) - \Phi^{(1)}_{\alpha\beta}(r) - \ln\left[1 + \frac{e^{f_{\alpha\beta}(r)(\gamma_{\alpha\beta}(r) - \Phi^{(2)}_{\alpha\beta}(r))} - 1}{f_{\alpha\beta}(r)}\right] \tag{3.20a}$$

$$g_{\alpha\beta}(r) = e^{-\Phi^{(1)}_{\alpha\beta}(r)}\left[1 + \frac{e^{f_{\alpha\beta}(r)(\gamma_{\alpha\beta}(r) - \Phi^{(2)}_{\alpha\beta}(r))} - 1}{f_{\alpha\beta}(r)}\right] \tag{3.20b}$$

where $\Phi^{(1)}_{\alpha\beta}(r)$ and $\Phi^{(2)}_{\alpha\beta}(r)$ are respectively the repulsive and the attractive parts of the potential, defined by

$$\Phi^{(1)}_{\alpha\beta}(r) = \begin{cases} \Phi_{\alpha\beta}(r)(r) - \Phi_{\alpha\beta}(r)(r_{min}) & if r < r_{min}; \\ 0 & otherwise. \end{cases}$$

$$\Phi^{(1)}_{\alpha\beta}(r) = \begin{cases} \Phi_{\alpha\beta}(r)(r_{min}) & if r < r_{min}; \\ \Phi_{\alpha\beta}(r)(r) & otherwise. \end{cases}$$

3.3 BRIDGE FUNCTIONS AND MODIFIED-HNC or IMPROVED-HNC EQUATIONS

RHNC and MHNC EQUATIONS

Rosenfeld and Ashcroft[63] and Lado [64] proposed to solve the closure relation (3.12) with the Bridge functions of a reference hard- sphere system having a packing ratio optimized to give Thermodinamic Consistency. This approach is based on the assumption that the bridge functions at short range have a universal behaviour, for any potential, and thus they can adequately be represented by the bridge functions, in the PY approximation, of a hard-sphere system of a suitable density.

Two equivalent schemes were devised to enforce TC in the solution: one minimizes an expression for the free energy of the system (RHNC or Reference-HNC), and the other requires the equality of the compressibility computed from the equation of state (virial route) with that computed from the fluctuation route (Modified-HNC).

IMPROVED-HNC EQUATIONS and BRIDGE FUNCTIONS

It was realized by Ichimaru that non-universal features at medium range in the bridge functions could be important to describe the actual structure in some systems, i.e for the OCP at strong coupling. He obtained a formula[59] that relates the first term in the expansion (3.13) with the $h_{\alpha\beta}(r)$. Substituting in the expression (3.16) for $B^{(4)}$ the following approximations for the $c^{(3)}$

$$c^{(3)}(\mathbf{r}_1,\mathbf{r}_2,\mathbf{r}_3) = h(|\mathbf{r}_1-\mathbf{r}_2|)h(|\mathbf{r}_2-\mathbf{r}_3|)h(|\mathbf{r}_1-\mathbf{r}_3|) \tag{3.21}$$

one obtains

$$B^{(4)}(r) = -\frac{n^2}{2}\int h(r_1)h(r_2)h(|\mathbf{r}_1-\mathbf{r}_2|)h(|\mathbf{r}_1-\mathbf{r}|)h(|\mathbf{r}_2-\mathbf{r}|)\,d\mathbf{r}_1\,d\mathbf{r}_2 \tag{3.22}$$

The corresponding expression for the first term $B^{(4)}$ in a two component system is

$$B^{(4)}_{\alpha\beta}(r) = -\frac{1}{2}\sum_{\gamma\delta}\int h_{\alpha\gamma}(r_1)h_{\alpha\delta}(r_2)h_{\gamma\delta}(|\mathbf{r_1}-\mathbf{r_2}|)h_{\gamma\beta}(|\mathbf{r_1}-\mathbf{r}|)h_{\delta\beta}(|\mathbf{r_2}-\mathbf{r}|)\,\mathrm{d}\mathbf{r_1}\,\mathrm{d}\mathbf{r_2} \tag{3.22a}$$

Ichimaru and Iyetomi[65] solved the closure relation using bridge functions determined through these relations, where the total correlation function h(r) of the HNC solution were used. They rescaled the computed function at low r in order to reproduce the 'universal' repulsive behaviour at short distances and obtained a certain degree of thermodynamic consistency. They named this approach improved-HNC, as it starts from the knowledge of the HNC solution to evaluate the approximate bridge function used to obtain the improved solution.

CROSSOVER APPROXIMATION FOR THE BRIDGE FUNCTIONS

An approximation that retains both the universal behaviour of the bridge function at low r, that allows to reach Thermodynamic Consistency, and the structural information present in the $B^{(4)}$, was employed by Pastore Ballone and Tosi in an extensive work on the structure and the thermodynamics of molten salts [66]. Its is based on the idea of interpolating between the short range behaviour of the HS bridge functions, and the values given by $B^{(4)}$ at intermediate distances. A similar idea have been used in a work by Ashcroft, Foiles and Reatto [67], who interpolated between the 'universal' behaviour at short range, and the expression given by the MSA at long range.

The crossover between the Hard-spheres bridge functions and $B^{(4)}_{\alpha\beta}$ has the following form

$$B_{\alpha\beta}(r) = [1 - f_{\alpha\beta}(r)]\, B^{(4)}_{\alpha\beta}(r) + f_{\alpha\beta}(r) B^{HS}_{\alpha\beta}(r) \tag{3.23}$$

where the $f_{\alpha\beta}(r)$ is the mixing function that specify the region in which one

observes the crossing from the behaviour of one function to that of the other. We chose here for our work the same form chosen in ref.[66] that is

$$f_{\alpha\beta}(r) = \exp-(r/\xi_{\alpha\beta})^2 \tag{3.24}$$

where $\xi_{\alpha\beta}$ are the parameters that determine the crossover region and have been fixed by the position of peaks in the HNC result for $g_{\alpha\beta}(r)$.

The thermodynamic consistency is to be enforced by the appropriate choice of the parameters of the reference HS-system. We used as HS bridge functions those determined by a numerical solution of the PY closure for a reference system of hard spheres with the same ratio of diameters $d_{\alpha\alpha}/d_{12}$ as the ratio in the the peaks' positions of $g_{\alpha\beta}(r)$ in the HNC solution. In this way we have only one parameter d_{12} to vary to look for Thermodynamic Consistency.

The inverse isothermal compressibility $1/k_BT\chi_T\rho = \frac{\delta\beta P}{\delta\rho}|_T$ was calculated from the fluctuation route from the formula

$$\frac{\delta\beta P}{\delta\rho}|_T = 1 - n\sum_{\alpha}\sum_{\beta} x_\alpha x_\beta \tilde{c}_{\alpha\beta}(k=0) \tag{3.25}$$

while the inverse compressibility from the virial route where determined by numerical differentiation of the virial equation of state $\frac{\beta P}{\rho}$ repeating the calculation at a slightly higher value of density.

$$\frac{\delta\beta P}{\delta\rho}|_T \approx \beta\frac{\Delta\beta P}{\Delta\rho} \tag{3.26}$$

We used $\rho_1/\rho_0 = 1.002$. For the solution at higher density also the density of the reference system have to be varied in accordance, and also $B^{(4)}$ have to be scaled by the density factor that appears in front of the integral.

The scheme employed, that we call TC-IHNC consist in solving the HNC, calculating the bridge function $B^{(4)}$ from formula (3.22a) and use the resulting crossover with the hard sphere part, according to (3.23) to find a new solution.

As we shall show later, we explored the self consistency of the solution computed, by calculating again from it a new bridge function and a new solution.

3.4 NUMERICAL METHODS : BRIDGE FUNCTIONS AND INTEGRAL EQUATIONS

SOLUTION OF THE INTEGRAL EQUATIONS

The integral equations for the HNC and the TC-IHNC were solved using the Algorithm of Gillan[1]. It consists of a mixed iterative Newton-Rapson Method that is rather stable and accurate, and do not require as many iterations as a pure iterative methods. It projectes the unknown function onto a small basis, to represent its coarse shape. This part gives rise to system of nonlinear coupled algebraic equations that can be solved by a Newton-Rapson method. The fine variation of the function is then determined iterating the coarse solution in the integral equations. The cicle is repeated until convergence in the solution is attained.

We used in the calculations 512 points for doing the fourier transforms involved in the algoritm, with a mesh in real space of $\Delta r = 0.02a$, and we employed 9 basis functions over which the $\gamma_{\alpha\beta}(r)$ were projected to obtain the coarse part. Particular care as to be exercised in the treatment of the hard core discontinuity in the $g_{\alpha\beta}(r)$ that is determined by both the value of the potential and the bridge function at contact.

NUMERICAL EVALUATION OF THE BRIDGE FUNCTIONS

In order to evaluate numerically the integral in formula (3.22) one has to expand the terms $h_{\alpha\beta}(|\mathbf{r_1} - \mathbf{r_2}|)$ appearing in it in legendre polynomials so that one can carry out explicitely the angular integration, ending up with a sum of two dimensional integrals over 2 functions $h(r)$ and the product of the three coefficients

in the legendre polynomials expansion, where the sum runs over the order of the polynomial. This procedure is described in detail in ref.[2]. Other three integrations have to be carried out in order to compute the coefficients of the expansion, and this has to be done for every combination of the mutual position of the four points entering in the definition of the diagram. We carried out the numerical determination of the coefficients with the help of a finite transform, derived by a gauss-legendre integration formula. We used from 40 up to 80 points in this integration. The external bidimensional integration was carried out by a trapezoidal rule using from 101 to 141 points. It was necessary to include up to the 18th order in the legendre expansion. The accuracy of the algoritm is mainly determined by the accuracy in the determination of coefficients of the legendre expansion. In order to achieve the best accuracy in this integration it is necessary to transform a $g(r)$ that is not discontinuous, at contact and to subtract from the transformed function a contribute with an analitic formula, as indicated in the reference.

Tests were made employing the same trapezoidal rule for all the integrations, and it resulted in serious errors in the determination of the bridge functions. This is directly connected to the presence of high and narrow peaks in the pair correlation functions. From basic numerical analysis one knows that the numerical integration of this kind of functions has to be done with particular care.

3.5 MONTE CARLO SIMULATION

The Monte Carlo Simulation used to compare the results from the integral equationstheory was reported by us in refs.[28]wl. We used a Canonical ensemble simulation with 64 atoms and 128 bond particles, in a cubic simulation cell of

lenght 9.2996 a, with periodic boundary conditions

We prepared the system in the position of a diamond-type lattice, as shown in fig 2.3 and equilibrated the system for 1.600.000 elementary moves, roughly 8.000 moves per particle, at $V^* = 1$, and then we made a series of runs at various coupling strenght equilibrating first the sistem for at least $\approx$ 8000 moves per particle and taking statistics on runs of the same lenght. During the run we monitored the energy, the pressure and the order parameter of (111) and (001) planes in order to be sure of the equilibration of the sample and to be sure that the sample was not undergoing crystallization. It appears that the correlation time between subsequent configurations in the simulation increases with coupling strenght. Thus the results at strong coupling present greater numerical uncertanties. In particular this slowing down changes with the values of the diameters, and for the parameters reported as set 3 we could not perform a simulation in a resonable time. This could be improved allowing a kind of move that samples the configuration space better than the usual one, by allowing bond breaking and forming processes that change the number of bonds in the system.

Chapter 4

Results

4.1 LIQUID GERMANIUM

LOCALIZATION OF BOND PARTICLES AND STRUCTURAL TRENDS

First we examine here the behaviour of the LAM model at costant density on varying the temperature, i.e. on increasing the coupling strenght V^*, as results from the analysis of structural trends in the partial pair correlation functions and structure factors. Our major aim in this presentation is to follow the process of localization of bond particles in bonds and to show that the degree of BP localization induce increasing directionality in the effective atom-atom interaction, leading to peculiar features in the structure. The calculations reported here were made solving the model in the liquid state by means of the HNC-integral equations, at a density and values of parameters, reported in table 2.1 as set 1, appropriate to liquid germanium.

On increasing the coupling strenght, the atomic component A manifests a strong attraction to the BP component through the potential well present on its surface (see fig. 2.4), and one can gauge the degree of BP localization in this well from the values assumed by the main minimum of the pair correlation function $g_{AB}(\mathbf{R_{AB}})$ (see fig. 4.1). A main sharp minimum with value zero in this function,

together with a first narrow and quite high peak signals the creation of a well defined first coordination shell of BP around each A atom, and a slow exchange of particles from this shell with the rest of the fluid. In this sense we can say that these BP are temporary **localized** in the potential well at the surface of the A particle, the coordination number $N_{\alpha\beta}(R)$ being the number of BP trapped in it. They thus provide a preferred site of attraction to another A particle, that can form a bond by sharing the bond particle. This is what we mean saying that the model shows **association**. Directionality in the resultant A-A interaction is enforced when four BP are localized around that atom.

Figure 4.2 shows the partial pair distribution functions and the partial structure factors for coupling strenght V^* equal to zero. These results can be compared with liquid structure in additive models for mixtures of hard spheres with very different diameters, for both neutral fluids[44] and charged fluids[3]. In both these cases, some degree of relative order of the two components is marked by a valley in $S_{AB}(k)$ in approximate corrispondence with the main peak in $S_{AA}(k)$, while $S_{BB}(k)$(the structure factor of the small-sized component) is essentially featureless. As is evident from fig. 4.2, our choice of σ_{BB} by a tetrahedron rule (see formula 2.1) builds sharp structure in $S_{BB}(k)$and in $g_{BB}(r)$, while it preserves and somewhat strengthens the relative order of the two components. Localization of BP is nevertheless absent.

Figure 4.1, starting from the A-B and A-A pair distribution function at $V^* = 0$, illustrate how localization of bond particles proceeds on increasing V^*, and the structural changes that it induces in the atomic component, down to strongly supercooled ($V^* > 7.5$) liquid states.

Bond particle localization starts to appear at ($V^* = 2$) and grows rapidily, with the exchange of bond particles between localized states and free states being rapidly

suppressed and the atom-bond coordination number increasing towards 4. This is signalled at ($V^* = 2$) by the rapid drop in R_{AB} and N_{AB}.

From $V^* = 2$ to $V^* \approx 5$ the potential well acts mainly as an ordering interaction between the components, as only g_{AB} is affected, showing the formation of well defined shells of BP around A atoms by a rapid drop in the value attained at its main minimum. Thus we can say, in a pictorial way, that in this range of couplings there is a certain amount of association of A atoms, although exchange of bond particles with the surrounding liquid is still consistent ($g_{AB} \approx 0.8 - 0.3$) and doesn't allow the formation of bonds with a lifetime longer than the characteristic time needed for diffusion.

The next rapid change in structural behaviour occurs for V^* in the range 6-7. Here the localization of BP becomes quite strong ($g_{AB} \approx 0.1$), as its also shown by the appearence in g_{AB} of a quite sharp and high first peak, with an height of ≈ 10 (to be compared with the value of 3 at $V^* = 0$) right at the position of the well minimum. This means that rather stable (with respect to the characteristic time of diffusion) bonds are forming between A atoms, the number of bonds being roughly proportional to $N_{\alpha\beta}(R)$, with an average of 3 bonds for each atom. The fact of having three BP localized **on average** means that there is a certain amount of atoms which have got four BP, and can form a number of bonds from 2 to 4. At this point a strong directionality in the Atom-Atom interaction is present for those atoms that are fourfold coordinated to BP. This is apparent in the changes occurring in g_{AA}, where the first coordination shells splits, with the appearence of a structure that grows on increasing coupling to constitute a second peak just in the place where the pair correlation function showed a minimum at $V^* = 0$. This is marked in fig. 4.1 by the sudden drop in the position of the main minimum R_{AA} at $V^* \approx 8$. The ratio between the position of this second growing peak, that

develops in strongly supercooled states, and that of the main peak ranges from 1.5 and 1.6, and it compares well with the ratio between first and second neighbor atomic distance in a tetrahedrally bonded structure, that is the ratio between the edge of the tetrahedron and the lenght of the A-A bond (see fig 2.4) $\sqrt{\frac{8}{3}} = 1.63$. Upon further increase of V^* the coordination number N_{AB} slowly moves towards the value 4, while the localization of BP becomes essentially complete.

We can see from fig. 4.3 how the structural trends that we have followed from the pair correlation functions are reflected in the partial structure factors, on increasing coupling. Upon incipient localization of BP at $V^* \approx 2$, the valley in $S_{AB}(k)$ is shifted towards the position of the main peak in $S_{BB}(k)$, and a pre-peak grows in correspondence with the main peak in $S_{AA}(k)$. These features, together with the increasing depth of the valley, mark the increasing ordering between the components illustred above.

More remarkable is the behaviour of the atom-atom structure factor $S_{AA}(k)$ that first becomes slightly asymmetric (V^* up to 5), then developes a shoulder at its right side for V^* in the range 6-7.5, where the splitting of the first A-A coordination shell occurs. On further increase this shoulder grows into a strong peak at essentially unshifted position, while the former main peak is reduced to a pre-peak at progressive lower wavenumbers.

We want to compare these trends with those observed experimentally in liquid germanium. A well known qualitative feature of the observed structure factor of liquid germanium is the presence of such a shoulder near freezing, becoming an asymmetry in the peak shape at higher temperatures[46]. In figure 4.4 we show the structure factors for liquid germanium above freezing and amorphous germanium at room temperature from neutron diffraction experiments[10,48], plotted in reduced units ka (a being related to the number density n of the atomic compo-

nent by $a = (1/4\pi n)$, for comparison with fig. 4.3. As we can see in detail in the following sections we can make contact with the observed structure for the liquid near freezing and the result at ($V^* = 7.5$) while the structure of the supercooled liquid at $V^* \approx 20 - 24$ qualitatively resembles that observed in amorphous germanium.

QUANTITATIVE COMPARISON WITH EXPERIMENT

The partial structure factor of the model $S_{AA}(k)$ should be directly compared to the structure factor of Germanium as measured by neutron diffraction, as they are scattered only by the "atomic" component (scattering off nuclei), while X-ray are also sensitive to the electronic component. In a previous work [28] we made the comparison between the structure factor displayed by the model at $V^* = 7.5$ and the X-ray scattering data of Waseda[9], which were the only accurate data available to us in numerical form[11] at that time. Now accurate neutron scattering data are available from the experiment of Salmon[10], thus we can compare our model directly with them. Figure 4.5 shows the data from both X-ray e neutron scattering experiments compared with our results.

From the figure it's apparent that there are slight differences between neutron and X-ray data, mainly in the height and the position of the first peak and its shoulder, and a little dephasing of the oscillations at high values of k. This difference can be only partially accounted for by the different data reduction algoritms employed in the two experiments, and should be attributed to the contribution of valence electron to the observed X-ray diffracted intensity[4].

From the figure we can see that there is a good qualitative agreement between our results and experiment, but we also notice that differences between the model's structure factor and the neutron scattering result amount to a scale factor. Then

our result for $S_{AA}(k)$, contracted of a factor 1.037, were compared to the same neutron scattering data, and now the model fits quite well not only the first peak but also the overall shape of the observed results. Such a comparison is shown in fig. 4.6 for the partial structure factor $S_{AA}(k)$.

Thus in order to account for the experimental results in a quantitative way, we should repeat our calculation with values of the hard-sphere diameter A-A in reduced units $\sigma^*_{AA} = r_{AA}d/a$ (where r_{AA} is the value expressed in the first column of tab 2.1 and a is related to the density as explained in the previous section) enhanced by the factor 1.037. If we fix the bond lenght as $d = 2.68\mathring{A}$ from Salmon's experiment, descarding the previous value $d = 2.63\mathring{A}$ quoted in table 2.1, we need a density of $n_{Ge} = 0.0479\mathring{A}^{-3}$, that is 5% higher than the value of $0.0456\mathring{A}^{-3}$ found from experiment.

In conclusion the density required for the model to be in agreement with the diffraction data, once we have taken the bond lenght from the same experiment, is higher than the experimental density of Ge. As the equilibrium density of a fluid at a given pressure is the result of a delicate balance between repulsive and attractive forces, is not strange at all that the rough schematization of repulsive interactions made in the model doesn't allow to predict the correct equilibrium density. It requires the adoption of more realistic repulsive potential to predict also the correct equilibrium density of Germanium.

We proceeded further on, asking weather the solution of the model by a more accurate approximation than the HNC closure could further improve the agreement with experiment. We employed the scheme outlined in sec. 3.3 , already used with succes in previous work on molten salts[66],and we solved the integral equations derived from the closure relation (3.12). The bridge functions were determined as a crossover (see eq.3.23,3.24) between the bridge functions of an

hard-spheres reference system (found in the PY approximation), and the first term in the espansion (3.13) $B^{(4)}_{\alpha\beta}(r)$ computed by the integral in formula (3.22a) using as input the total correlation functions $h_{\alpha\beta}(r)$ of the HNC-solution. The mixing parameters $\xi_{\alpha\beta}$ where fixed at the main peak's position in the HNC solution. The ratio of diameters d_{11}/d_{12} and d_{11}/d_{12} for the hard-sphere reference system was fixed as well from the ratio in the peak's position. The only free parameter d_{12} was varied to enforce Termodinamic Consistency (TC) between virial and fluctuation compressibility. From the solution obtained (I iteration) we computed again $B^{(4)}_{\alpha\beta}(r)$ and solved again the integral equations with it, to obtain a new TC solution (II iteration).

This solution is show in comparison with the HNC solution and neutron scattering data in fig. 4.6, and one can see that indeed a better agreement in S(k) is reached. We can make it even better by choosing a coupling of $V^* \approx 6.5 - 7$, in order to have less a marked shoulder. In the same figure we show also the pair correlation function g_{AA} of the model in the HNC and in the TC solution compared to experiment, and we shall comment on it later, in the section dedicated to the accuracy of the integral equations method.

We can conclude this section by stating that this model can fit the structure factor of liquid Germanium as well as the hard- sphere system is known to fit the structure factors of simple liquid metals and alloys[44]. We think that a better modelling of the real system can be achieved using A-A interactions more realistic than hard sphere repulsions.

4.2 ACCURACY OF THE INTEGRAL EQUATION METHOD

We shall discuss here the work done to test the quality of the structural predictions made by the liquid-structure theory in the LAM, for values of coupling corresponding to liquid states down to values in the supercooled- liquid region, and our attempts to improve the approximations involved by the use of empirically-mixed closures or the inclusion of bridge functions, in order to predict the structure with the best accuracy.

At this purpose, we made some Monte Carlo simulations in the canonical ensemble of the LAM at different values of coupling ($V^* = 1$, 5, 7.5, 10, 14, 22) choosing the parameters of the model as set 2 in table 2.1, where the tetrahedron rule has been somewhat relaxed, and the density was fixed to a lower value than in the liquid near freezing (it is precisely the density of the compacted amorphous phase). This choice for the density and for σ_{BB} is motivated by the need to accelerate the equilibration rate and to reduce the lenght of the sampling runs in the simulation. Further details on the simulation were given in chap. 3. The localization process of bond particles shows the same features as shown before at liquid density, but the splitting of the first coordination shell, that is the emergence of a new closer second coordination shell appears before, at $V^* = 6 - 6.5$ with respect to $V^* = 7 - 7.5$ for parameters at liquid density.

Figure 4.7 shows the HNC and Monte Carlo results for $g_{\alpha\beta}(r)$ at two different values of the coupling strenght, $V^* = 5$ in the liquid region that correspond to the onset of strong association, and $V^* = 10$ in the supercooled region. It is seen that the HNC solution is still in full quantitative agreement with the simulation up to the value $V^* = 5$, except that the values (only partly shown in the figure) at hard-sphere contact, mainly in g_{AB}, are higher in the HNC. The TC solution found in the HMSA approximation is very similar to the HNC and to the data over this range of V^*.

On the other hand we found that from this value of V^* on, some quantitative discrepancies between HNC and simulation arise. Let's summarize with the help of the case $V^* = 10$, shown also in fig. 4.7, the other work done for greater couplings. We find in general that a good agreement between HNC and simulation persists up to large values of V^* for $g_{AB}(r)$, $g_{BB}(r)$, except for slight asymmetries in the first peak of $g_{AB}(r)$ and in II peak of $g_{BB}(r)$ (that show also a lower value) for the HNC solutions. However there is a discrepancy, increasing with coupling, for $g_{AA}(r)$ in that the HNC seriously underestimates the structure of its second peak, that is gives too high a value of the main minimum, and too low a value of the II peak. Thus the HNC poorly predicts the progressive formation of the second shell of neighbours arising from the correlations of two atoms bonded to the same atom.

This defect of the HNC approximation is not remedied by the HMSA, that in the supercooled region performs worse that the HNC, predicting even higher values of the main minimum; in addition it shows the disappointing feature of yielding a negative value for $g_{AB}(r)$ at its main minimum. A major drawback of the HNC approximation is shown in fig. 4.8 for the LAM at liquid density (set 1), in relation with the behaviour of the compressibility ξ_T evaluated from the fluctuation formula (3.25) and from the virial route, by numerical differentiation of the virial equation of state (see eq. 3.26). The increasing degree of thermodynamic inconsistency between the two routes showed by the HNC solution is evident from the fact that, while the virial compressibility increases only slowly up to $V^* \approx 20$, the fluctuation compressibility shows first a more rapid linear increase and then seems to diverge at values of $V^* \approx 22$ for the parameters quoted; the same behaviour is shown by the HNC solution at $V^* \approx 14$ for the parameters chosen in the Monte Carlo simulation (set2).

It seems that the HNC somewhat misplaces the location of the spinodal line between the liquid and the solid phase in the (ρ, P) thermodynamic plane, that is the loci of points in which the the second derivatives of the free energy with respect to volume (or density) is zero, lines at which the compressibility diverges and that marks the region of mechanical stability of the liquid state in the supercooled - metastable region. This prevents to obtain solutions in the HNC approximation for larger values of coupling in the supercooled region, due to the intrinsic sensibility to the value of the fluctuation compressibility shown by the numerical algorithm of solution, that becomes unstable when this value is high enough. It can be largely remedied by the adoption of any TC empirical-mixed closure like the HMSA or by the inclusion in the closure relation of the brige functions of hard spheres like in the thermodynamic consistent MHNC approach.

As we have assessed the importance of including the hard-sphere bridge function for the thermodynamic consistency, and in essence for the possibility of finding solutions for the LAM in the extreme supercooled region, we turn to the accuracy on the prediction of the structure. For this analysis we focused our attention on the LAM at the value $V^* = 7.5$, that in the simulation shows already some structure in the second peak of g_{AA}, solving for it the integral equations at the same value of the parameters used in the Monte Carlo simulation. The inclusion in the closure relation of hard-sphere bridge functions alone, acting like an effective short-ranged repulsive potential, mainly affects the values of $g_{\alpha\beta}(r)$ in the first peak region, giving lower values of the peak and slightly higher values of the main minimum, and cannot improve the agreement with simulation but at the first peak value. The other differences seen between the HNC solution and simulation arise mainly from the not-universal, not hard-sphere-like behaviour of bridge functions at intermediate range.

Thus we explored the effects on structure of the first term $B^{(4)}_{\alpha\beta}(r)$ in the density expansion of bridge functions, as expressed by formula (3.22a) and evaluated from the knowledge of $h_{\alpha\beta}(r)$ of the HNC solution, including it in the closure relation and solving then the resultant integral equation. Clearly the new evaluated $h_{\alpha\beta}(r)$ is different from the previous one, and gives rise to a different bridge function $B^{(4)}_{\alpha\beta}$. We reached self-consistency in this iterative process, and explored for the first time to our knowledge, whether the first iteration approximation is close to the self-consistent determination of $B^{(4)}_{\alpha\beta}(r)$. The iterative process was stopped when the difference between the old and new determined bridge function was comparable to the numerical accuracy of our algorithm for computing them from the $h_{\alpha\beta}(r)$.

The resulting structure for $g_{\alpha\beta}(r)$ at each iteration is shown in fig. 4.9 together with the bridge functions from the first and the fourth iteration; 4 iterations are enough to reach self-consistency with our criterion. The three bridge function are characterized by a marked first valley at the position of the peaks in $g_{\alpha\beta}(r)$, followed by a peak in the region of the main minimum. Let's analyze the consequences of these features on the structure. The effect of the bridge functions on g_{AB} and g_{BB} is to eliminate the residual discrepancies with the simulation, as one can see from fig. 4.10 where the self-consistent solution is compared to the simulation; the higher values at peaks and lower values at the main minimum could soon be put in agreement with the simulation once the hard-sphere-like behaviour at low r, here neglected, is taken into account; in g_{AA} the main minimum is predicted with the correct depth, but yet not at the correct position, and the structure of the second peak is greatly enhanced with respect to the HNC, but present a marked splitting of the second shell that is not present in the simulation data; further inclusion of the short range term worsen the agreement.

As the present determination of the bridge function was quite accurate, and the discrepancies are outside the statistical error in our simulation, we should conclude that they are entirely due to terms neglected in the scheme that replaces $B_{\alpha\beta}(r)$ with $B^{(4)}_{\alpha\beta}$ as given by formula (3. 18). To trace the origin of the remaining discrepancy, we should remaind now that $B^{(4)}(r)$ is only the first term in the expansion (3.13) of $B(r)$, whose expression is given in formula (3.15), involving the $c^{(3)}(\mathbf{r_1}, \mathbf{r_2}, \mathbf{r_3})$ and that the relation used by us (eq. (3.22), (3.22a)) can be derived from it making the approximation (3.21) Maybe that this simple factorization of $c^{(3)}$ is not completely accurate in our case. A more likely possibility is that higher order correlations are equally important, leading to some strong structures at intermediate range in higher order terms of the expansion (3.13). We shall give here an argument that strongly supports this conclusion.

The bridge functions $B^{(4)}_{\alpha\beta}$ take into account correlations between four particles, as one can see by the considerations of the diagram that correspond to the integral in the expressions (3.22), (3.22a).

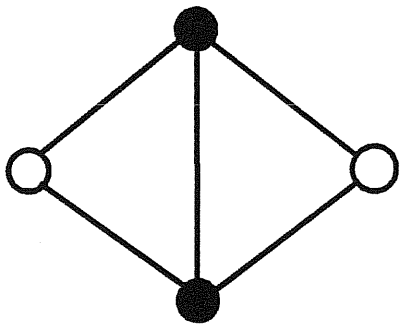

A line in this diagram gives the correlation between two particles as represented by the total pair correlation function $h_{\alpha\beta}(r)$, and black vertices represent variables to be integrated, namely $\mathbf{r_3}, \mathbf{r_4}$, while white vertices are the variables not integrated and $r = |\mathbf{r_2} - \mathbf{r_1}|$ gives the distance r at which the bridge func-

tion is evaluated. Now let's consider the kind of correlations present in a limiting case, that is is the solid phase. In the tetrahedral structure of the crystal are present rings of 6-atoms, and it is evident that similar correlations are also strong in the amorphous phase. These correlations in the ring are described by terms in the bridge function's expansion (3.13) of order higher than 4. To be precise they correspond to correlations involving up to six particles if the pair A-A or B-B are involved, and up to 12 particles if pairs A-B are involved. These terms are neglected in the approximations that retains only $B^{(4)}$.

The last point that deserves further investigation, and some work is in progress along this direction, is how a TC solution that mantain an accurate structural description can be obtained by the self-consistent $B^{(4)}_{\alpha\beta}$. Including the short range hard-sphere term at each stage in the iteration, as we attempted in the comparison with the experimental structure of liquid Germanium, is cumbersome, as convergence in the bridge functions becomes slower than before. A better compromise may be that of making a crossover of the self- consistent $B^{(4)}_{\alpha\beta}$ with the hard sphere-like part only at the end.

At the present stage of the investigation our conclusion is that the crossover with hard-sphere bridge functions must be handled with care, particularly with respect to $B^{(4)}_{AA}$, where less weight should be given to the short-range-repulsive part, with respect to the other components, if one want to reach the best accuracy attainable at this level. In particular one has to resort to more complicated ways of making the crossover than that employed here.

Turning again, after this discussion, to the comparison of the $g_{\alpha\beta}(r)$ for the LAM at liquid density with the experimental structure of germanium, fig. 4.11 shows the pair correlation function g_{AA} as obtained at the second iteration, mantaining the TC consistency request at each stage, and the corresponding bridge

function with the two terms that enter in the crossover expression. The fact that it behaves worse than the HNC in describing the main minimum region can be traced to an overestimation of the the hard-sphere-like short range contribution to the crossover.

4.3 STRUCTURE OF THE SUPERCOOLED STATES

We want to contrast here the results obtained in the LAM for high values of the coupling parameter V^*, to the experimental structure of amorphous Germanium. Usually amorphous Germanium is prepared by non-equilibrium techniques, like deposition from a gaseous phase onto a cold substrate. It's not possible to prepare it by fast cooling from the melt by usual fast-cooling-techniques[8], because it has a strong tendency to crystallize. Nevertheless one can think of obtaining it by pulsed laser tecniques as it was done for Silicon, by means of a short laser pulse that melts a portion of the solid, that is suddenly cooled very fast by the surrounding material. To this kind of experiment do correspond the simulation studies, made with various tecniques and potentials, quoted in the introduction. It's likely that a well annealed sample prepared by deposition tecniques tends towards the structure of a quenched 'glassy' material, that is essentially a system out of equilibrium because of long time-scale of its relaxation processes. Such a system is like a liquid with an arrested dynamics, and its average (spatial average) structure can be compared with the average structure of the ideal metastable-state of a supercooled liquid at the same temperature, as determined for example by the integral equations method. In this spirit, we make here such a comparison between a supercooled liquid and the actual structure of amorphous Germanium.

We saw in section 4.1 that the supercooled state of the LAM at liquid density

reaches an high degree of localization of BP, being the number of bonded atoms slightly smaller (N_{AB} being 3.7), with a number of atoms in the first coordination shell (not yet sharply distinguished from the arising second coordination shell, as one can see from the value at the main minimum of g_{AA} not yet zero) of ≈ 5. In order to make contact with the observed coordination number, one as to take into account the reduced density of Amorphous Germanium, and we solved the integral equations at this reduced density (set 3) in the HNC down to last value of coupling at which the HNC has solutions ($V^* = 22$). The high degree of association present in the system due to bonding of atoms, is signalled by the sharp, high first peaks in g_{AA} and g_{AB}, of values 13 and 25 respectively, to be compared with the value 3 of the hard shpere liquid at zero coupling strenght. The coordination number atom-atom N_{AA} now tends towards the value 4, while the bond-bond N_{BB} reaches the value 7, not too far from the value corresponding to a tetrahedral structure (N_{BB} =6).

In Fig. 4.12 we show the structure predicted by the HNC for $S_{AA}(k)$ and $g_{AA}(r)$ in comparison with the S(k) and g(r) from the neutron scattering data of Etherington[48]. The HNC result represent only qualitatively the features in g(r), with peaks in the correct positions but too low structure, and in S(K), the main discrepancy being the height of the first diffraction peak, and the position of the pre-peak. It's also evident the effect of the thermodynamic inconsistency, in the low k part, that can be remedied by the adoption of any TC closure, like in the case shown in fig. 4.3 for liquid densities, where the HMSA solution is illustrated, showing a better behaviour at low k, and a more marked separation between peaks than the HNC solution.

The next step was to use a bridge function obtained from the crossover betweeen a reference hard-sphere bridge function at low r and the $B^{(4)}_{\alpha\beta}$, determined

from the HNC solution. The partial pair correlation functions corresponding to the solution obtained in this way are displayed in fig. 4.13 together with the bridge functions employed. The comparison with experiment for S(k) (see fig. 4.12) shows that the structure of the pre-peak is better resolved, but the solution doesn't achieve yet quantitative accuracy. This is connected to the fact that the g(r) in the solutions determined until now with the integral equation method doesn't show a second peak clearly resolved from the first one. The pre-peak and the main peak in the structure factor essentially arise from the presence of the main peak and the second peak, that is from correlations connected to the short range tetrahedral order, as can be shown by back trasforming the g(r) truncated after the second minimum[48]. Thus the failure of integral equation method in providing an accurate descriptions of the second peak in g(r) explains its failure in providing an accurate description of the pre-peak position in S(k).

At the present state of our investigations it seems that only resorting to Monte Carlo simulations an accurate quantitative comparison with experiment can be attempted. A look at fig. 4.14, where we show the partial correlation functions obtained from the LAM at $V^*= 22$, from the Monte Carlo simulation with parameters as set 2, supports these conclusion, as one can see from the well defined shape of the second peak in g_{AA}, that reaches an height close to that observed in experiment, and is well separeted by the first peak by a deep minimum.

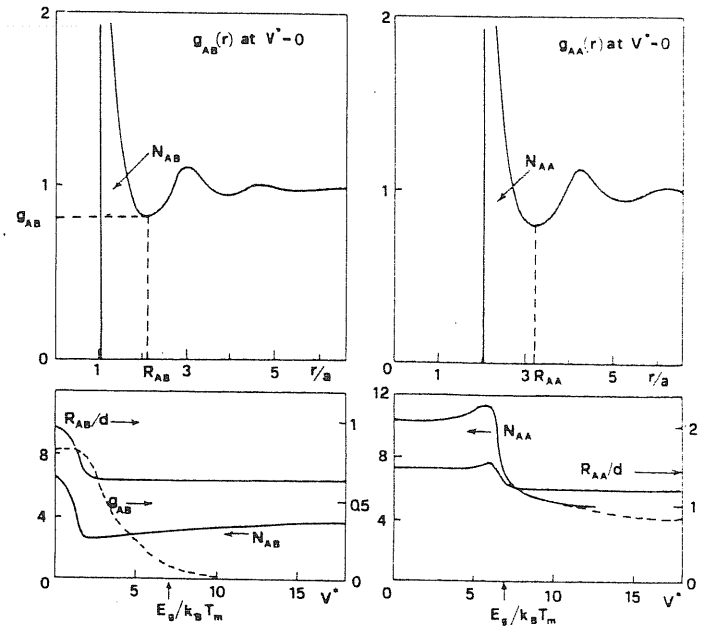

Fig. 4.1 – Schematic representation of bond particle localization and induced atomic structure changes with increasing coupling strenght V^* in the LAM. The top drawings show the atom-bond (left) and atom-atom (right) pair distribution functions at zero coupling strenght. The evolution of special features of these functions, as defined in the top drawings, is shown at constant liquid density in the bottom drawings. The dashed portion in the curve for N_{AA} shows the effect of reducing the density from that of freezing Germanium to that of compacted amorphous Germanium. The value $V^* = E_g/k_BT_m$ is marked on the bottom axes.

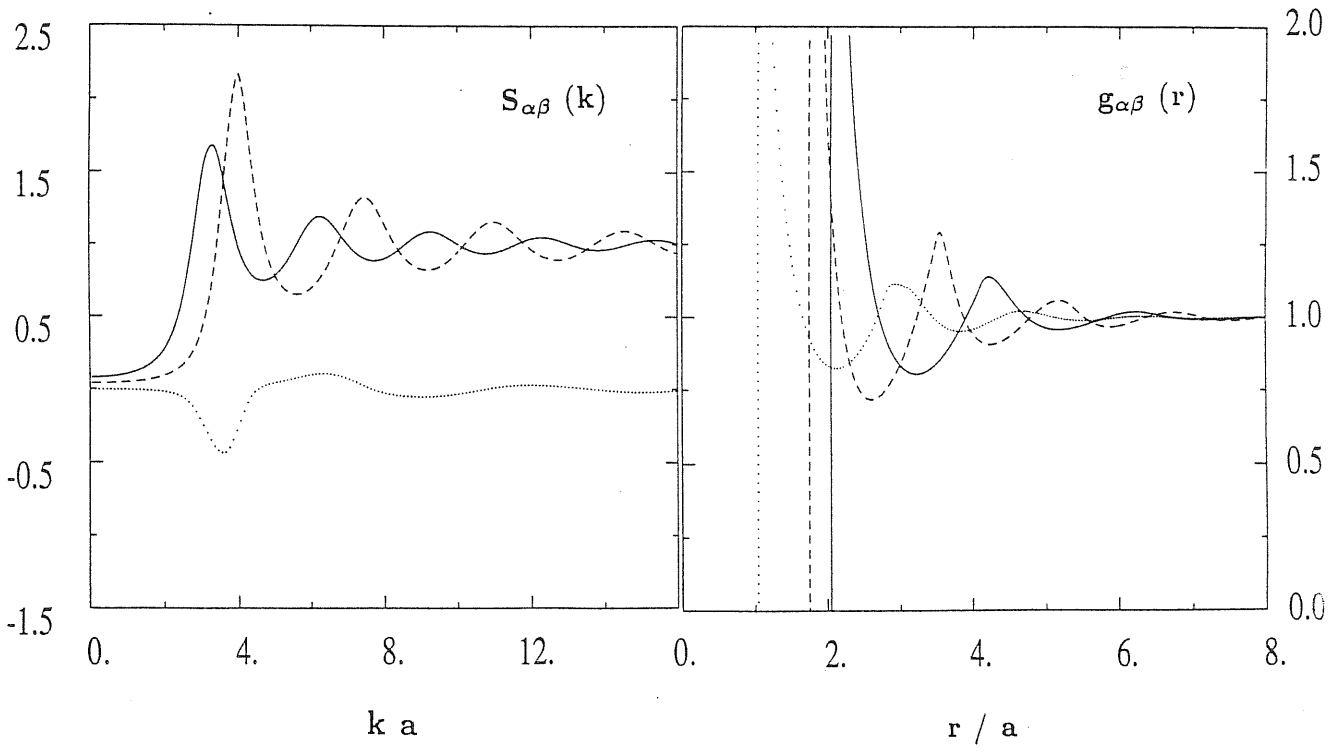

Fig. 4.2 – Partial structure factors $S_{\alpha\beta}(k)$ (left) and pair distribution functions $g_{\alpha\beta}(r)$ (right) for the LAM (set 1) at $V^* = 0$ in the HNC approximation. Full curves, A-A correlations; dotted curves, A-B correlations; broken curves, B-B correlations. Values of the peaks in $g_{\alpha\beta}(r)$ are: 3.65 (A-A); 3.04 (A-B); 6.02 (B-B).

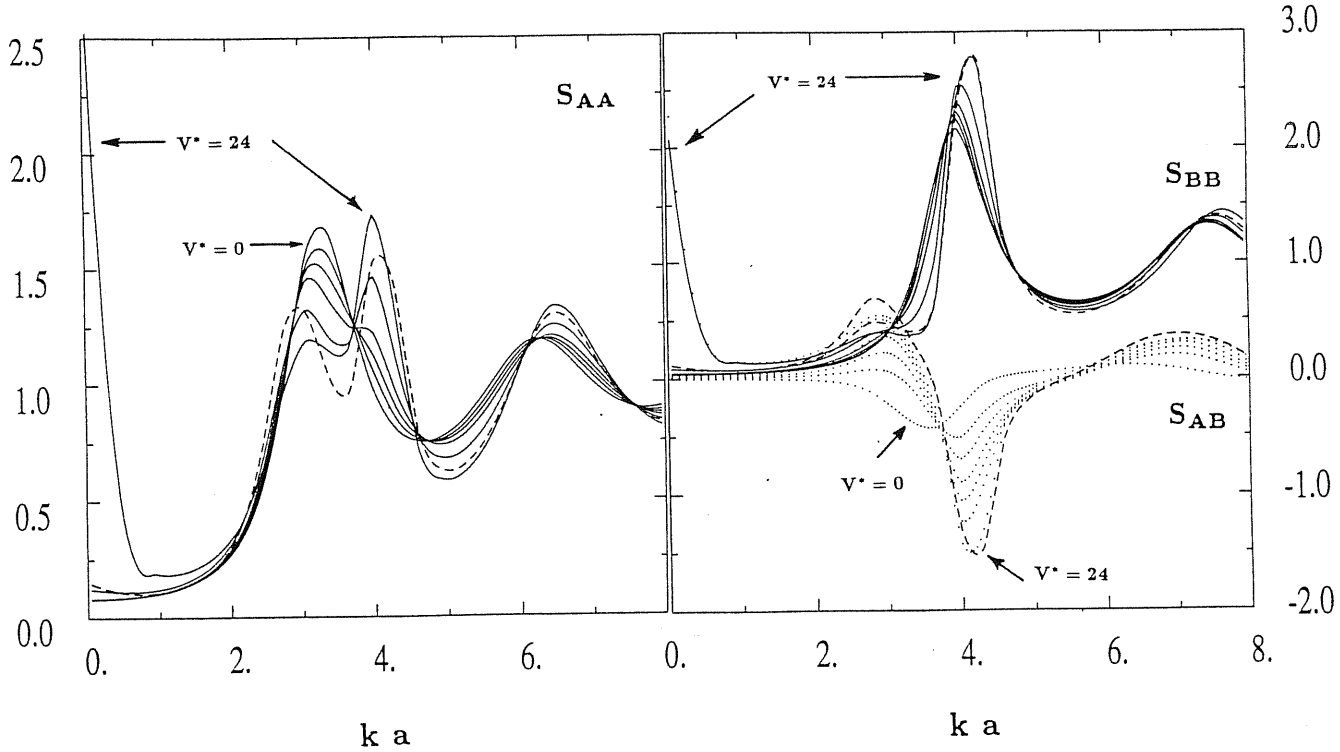

Fig. 4.3 – Partial structure factors $S_{AA}(k)$ (left), $S_{AB}(k)$ (right, dotted curves) and $S_{BB}(k)$ (right, full curves) for the LAM (set 1) in the HNC at a series of values of the coupling strenght V^* ($V^* = 0$, 3, 5, 7.5, 14, 24, the first and the last value being marked in the figures). The broken lines give the HMSA (with $b = 1$) results for $V^* = 24$.

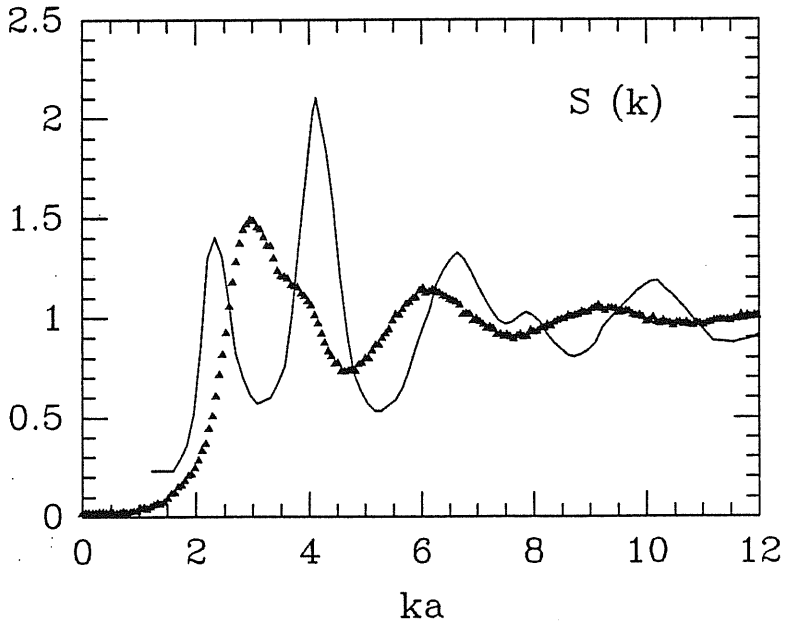

Fig. 4.4 – Structure factor S(k) of liquid Germanium near freezing (triangles) and amorphous Germanium at room temperature (solid line), in reduced units ka, from neutron scattering experiments. The scaling factor used are $a = 1.204$ for the liquid and $a = 1.229$ for the amorphous. Data are from the works of Salmon, ref.[ ] and Etheringhton, ref.[ ].

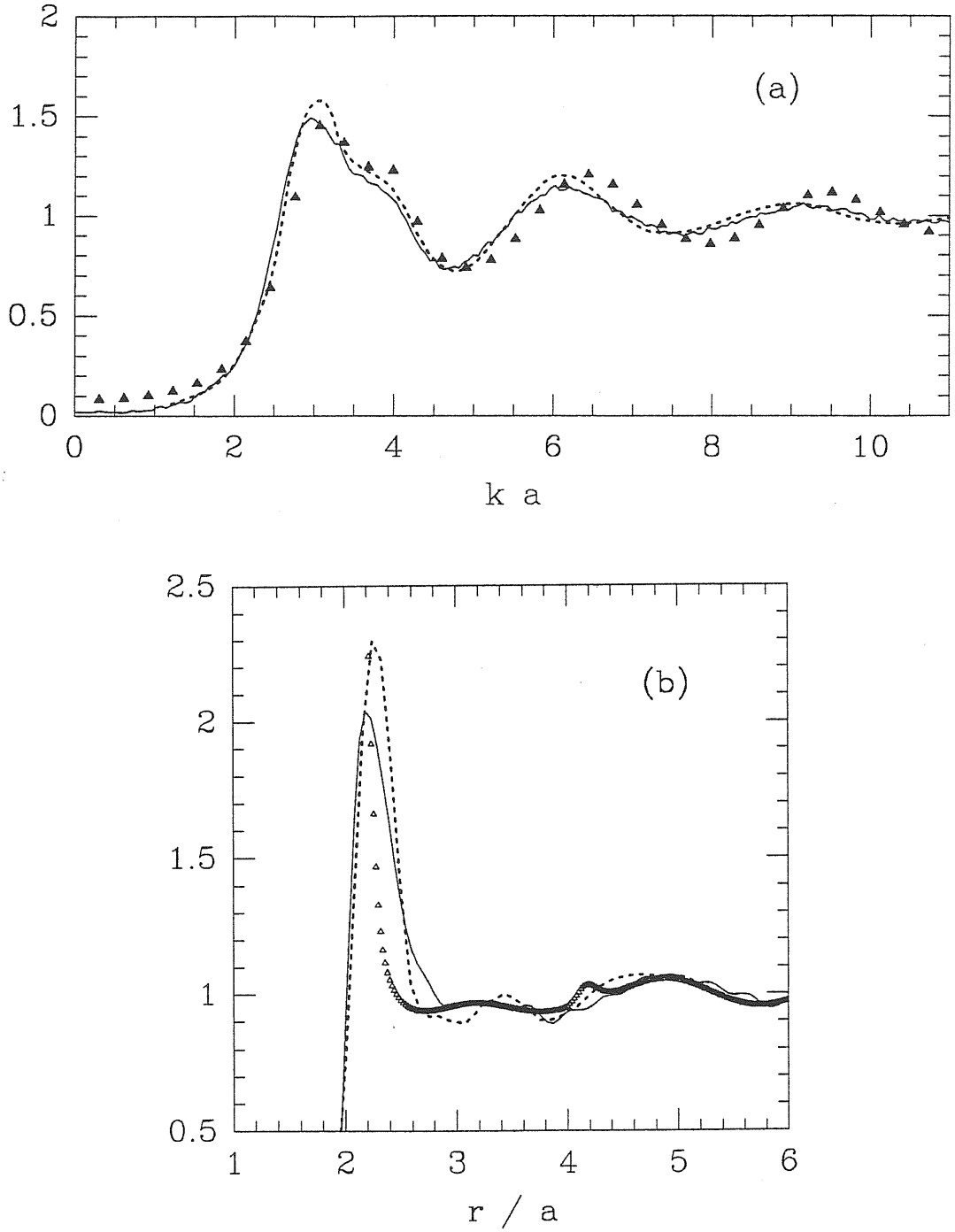

Fig. 4.5 – Partial structure factor $S_{AA}(k)$ (a) and pair correlation function $g_{AA}(r)$ (b) of the LAM in the HNC at $V^* = 7.5$ (triangles) and the experimental structure factor S(k) for liquid Germanium near freezing, in reduced units. Solid line, data from the neutron scattering work of Salmon, ref.[ ]; Dashed line, data from the X-ray scattering work of Waseda, refs.[,]. The scaling factor a is respectively 1.204 for the former and 1.200 for the latter.

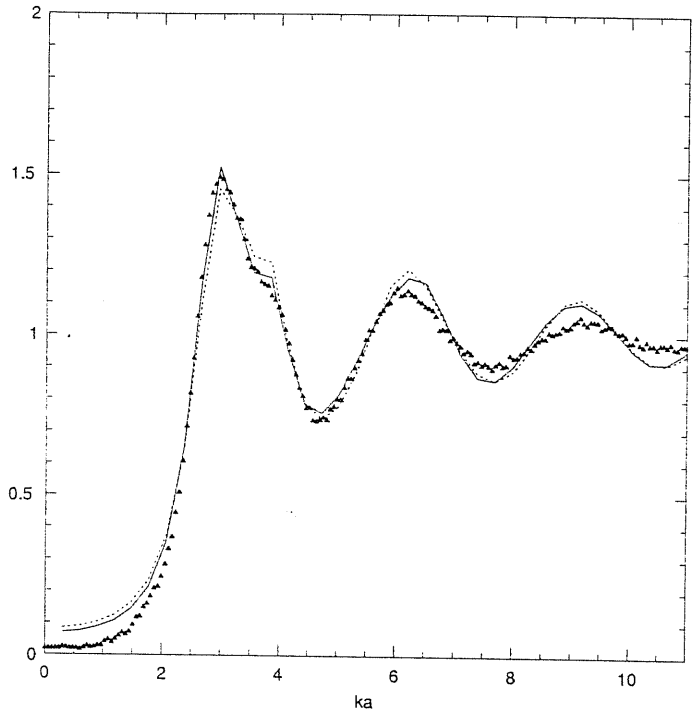

Fig. 4.6 – Partial structure factor $S_{AA}(k)$ of LAM in the HNC (solid line) and of the TC solution of the II iteration (dashed line) compressed by a factor 1.037, in comparison with neutron scattering data for liquid Germanium near freezing from ref.[ ], (triangles).

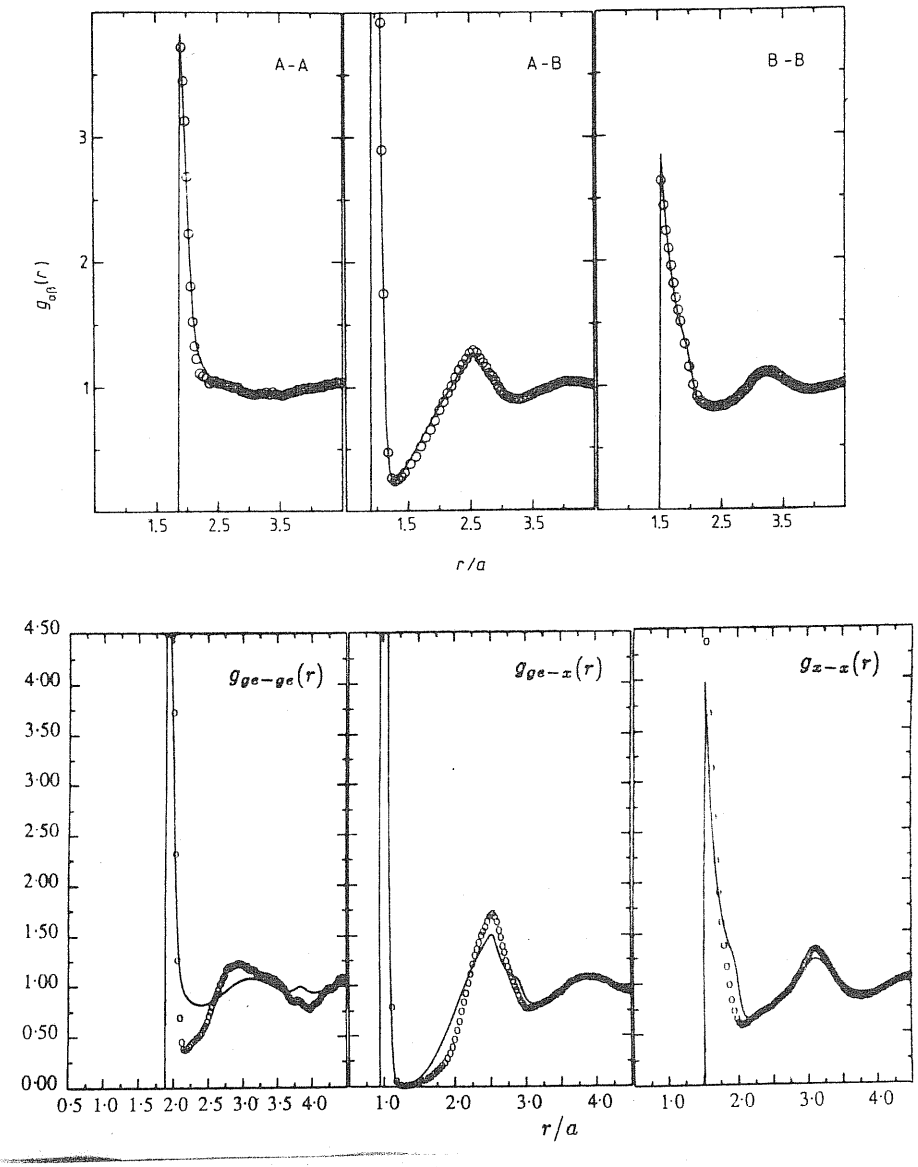

Fig. 4.7 – Partial pair distribution functions $g_{\alpha\beta}(r)$ in the LAM (set 2) at coupling $V^* = 5$ (upper figure) and $V^* = 10$ (lower figure). Full lines, HNC results; circles, Monte Carlo results.

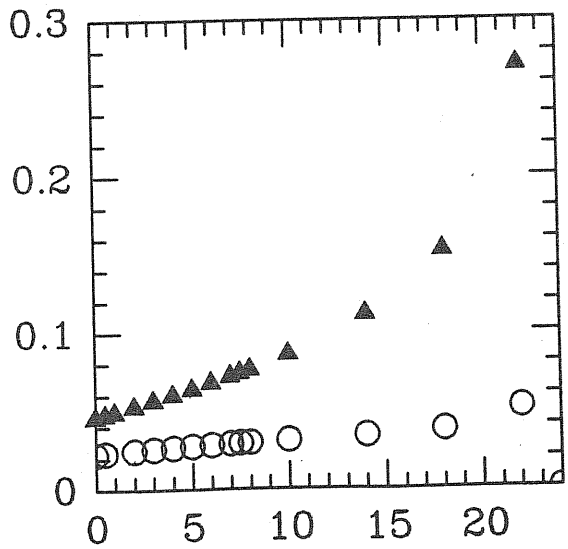

Fig. 4.8 – Thermodynamic inconsistency of the HNC solution for the LAM (set 1). Circles, Virial compressibility; triangles, Fluctuation compressibility.

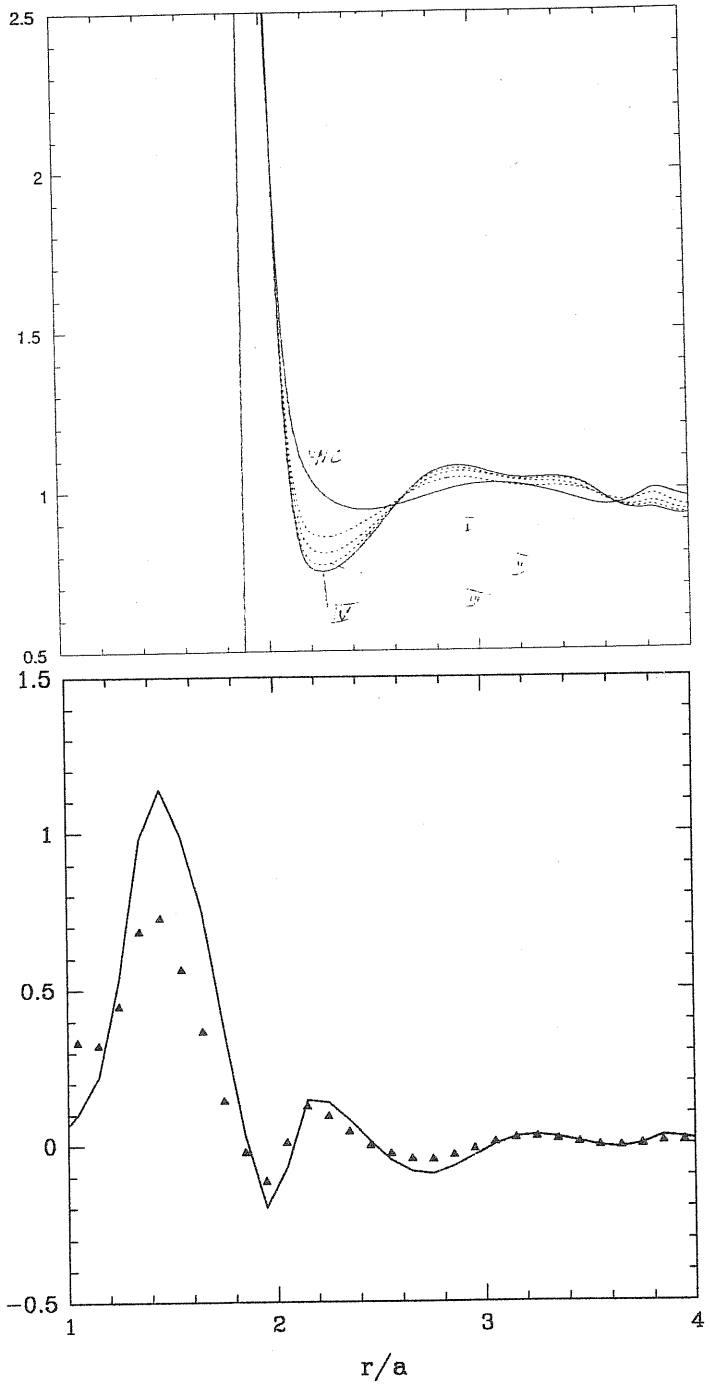

Fig. 4.9a – Convergence in the self-consistent solution. upper figure: pair correlation functions g_{AA} in the LAM (set 2) at $V^* = 7.5$; dotted line, HNC solutions; solid line, solution at the IV iteration; dashed lines, solutions at the I, II and III iterations. Lower figure: bridge functions $B^{(4)}_{AA}(r)$. Triangles, bridge calculated from the HNC solution. Solid line, bridge function at convergence.

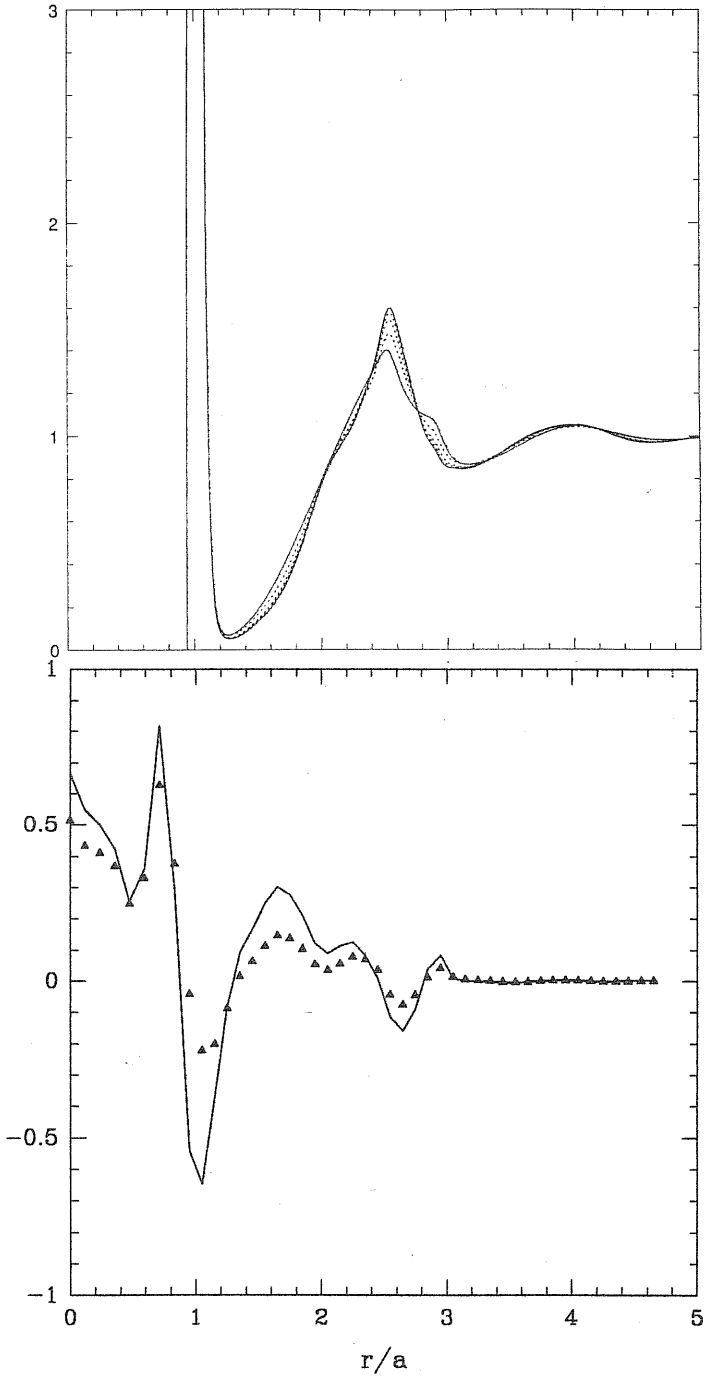

Fig. 4.9b – Convergence in the self-consistent solution. upper figure: pair correlation functions g_{AB} in the LAM (set 2) at $V^* = 7.5$; dotted line, HNC solutions; solid line, solution at the IV iteration; dashed lines, solutions at the I, II and III iterations. Lower figure: bridge functions $B^{(4)}_{AB}(r)$. Triangles, bridge calculated from the HNC solution. Solid line, bridge function at convergence.

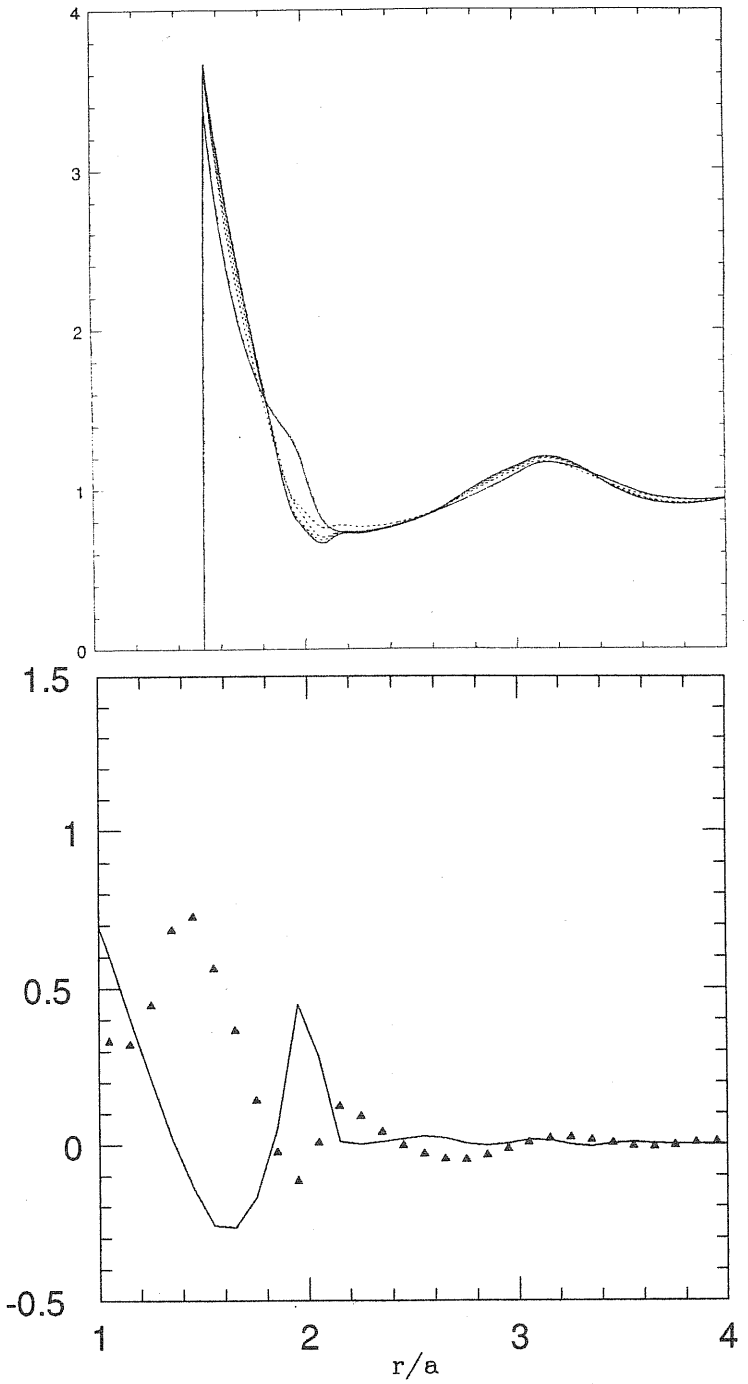

Fig. 4.9c – Convergence in the self-consistent solution. upper figure: pair correlation functions g_{BB} in the LAM (set 2) at $V^* = 7.5$; dotted line, HNC solutions; solid line, solution at the IV iteration; dashed lines, solutions at the I, II and III iterations. Lower figure: bridge functions $B^{(4)}_{BB}(r)$. Triangles, bridge calculated from the HNC solution. Solid line, bridge function at convergence.

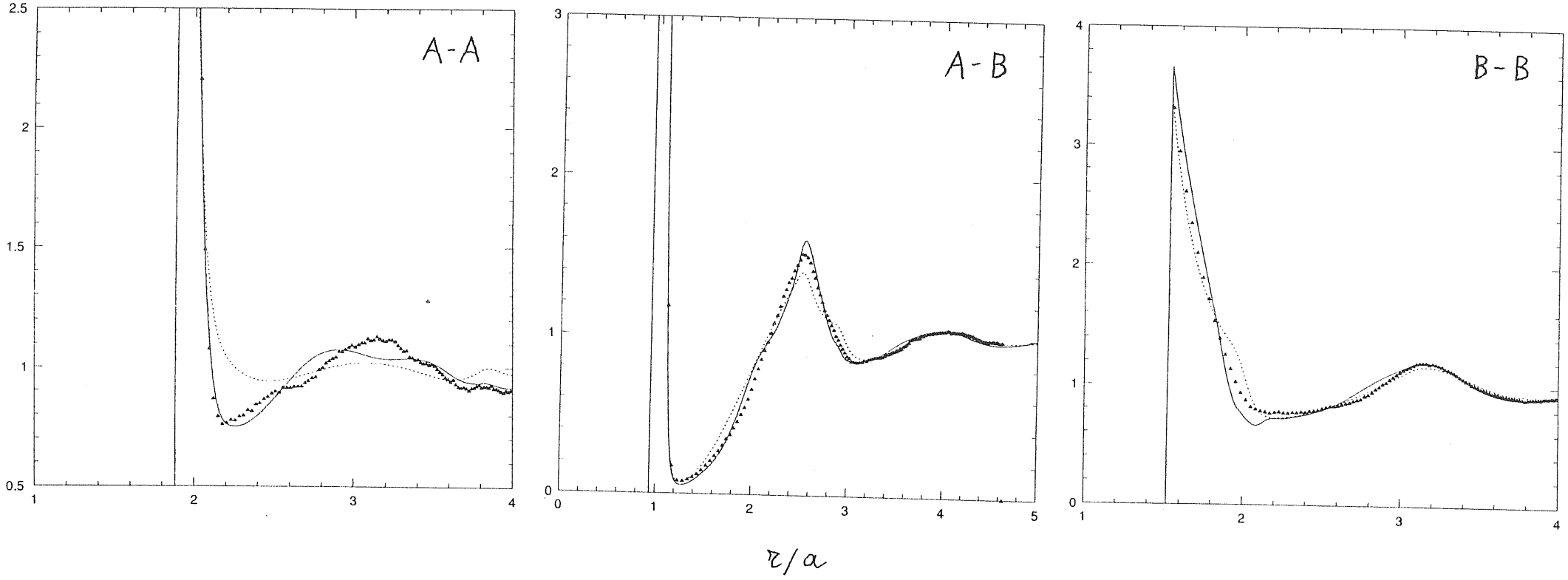

Fig. 4.10 — Partial pair distribution functions $g_{\alpha\beta}(r)$ in the LAM (set 2) at coupling $V^* = 7.5$. Triangles, Monte Carlo results; dotted line, HNC results; solid line, self-consistent solution with only $B^{(4)}_{\alpha\beta}(r)$

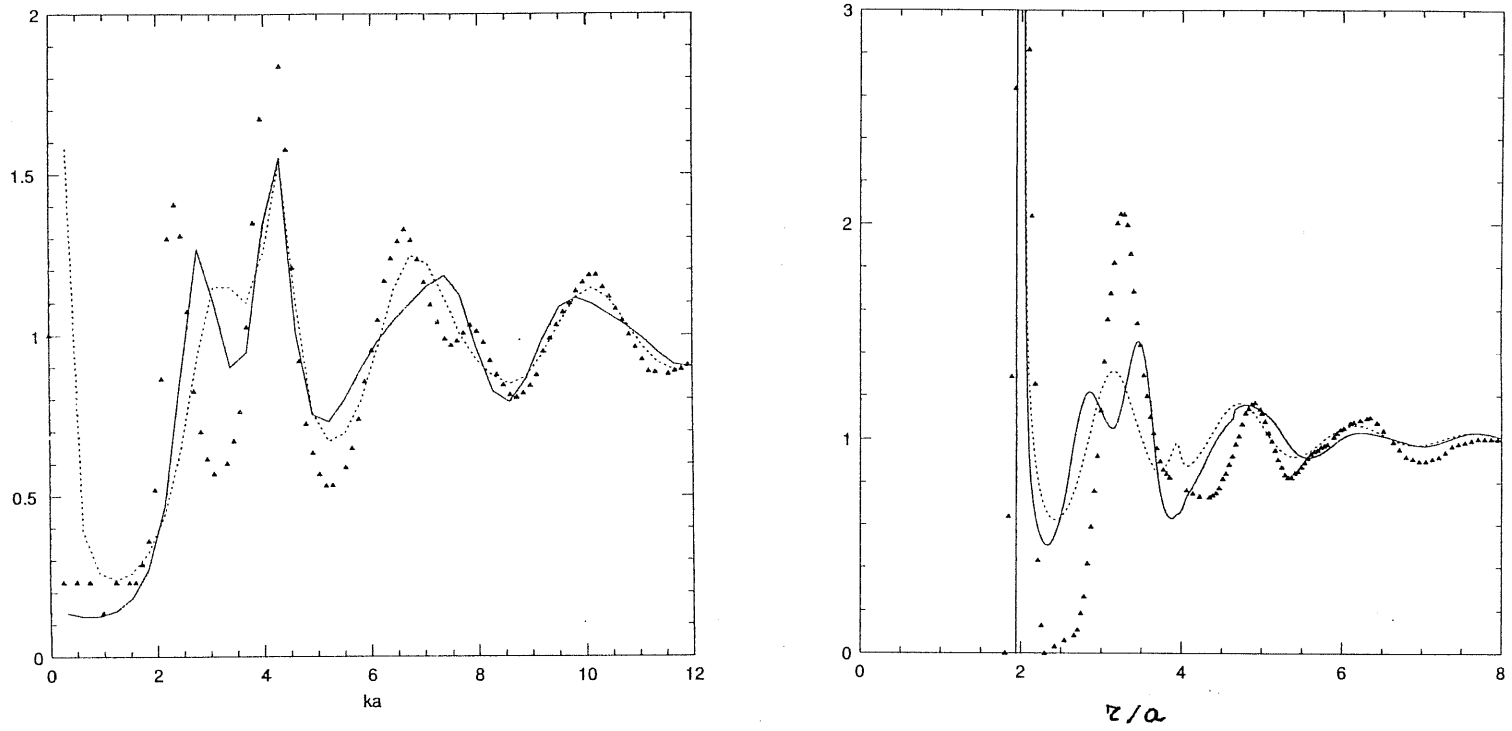

Fig. 4.11 — Structure factor $S_{AA}(k)$ (left) and pair correlation function $g_{AA}(r)$ (right) of the LAM (set 3) at $V^* = 22$ and the experimental structure factor S(k) for amorphous Germanium (triangles), in reduced units. Solid line, TC solution (see text); dashed line, HNC solution. Data are from the neutron scattering work of Etherington, ref.[ ]. The scaling factor a is 1.229.

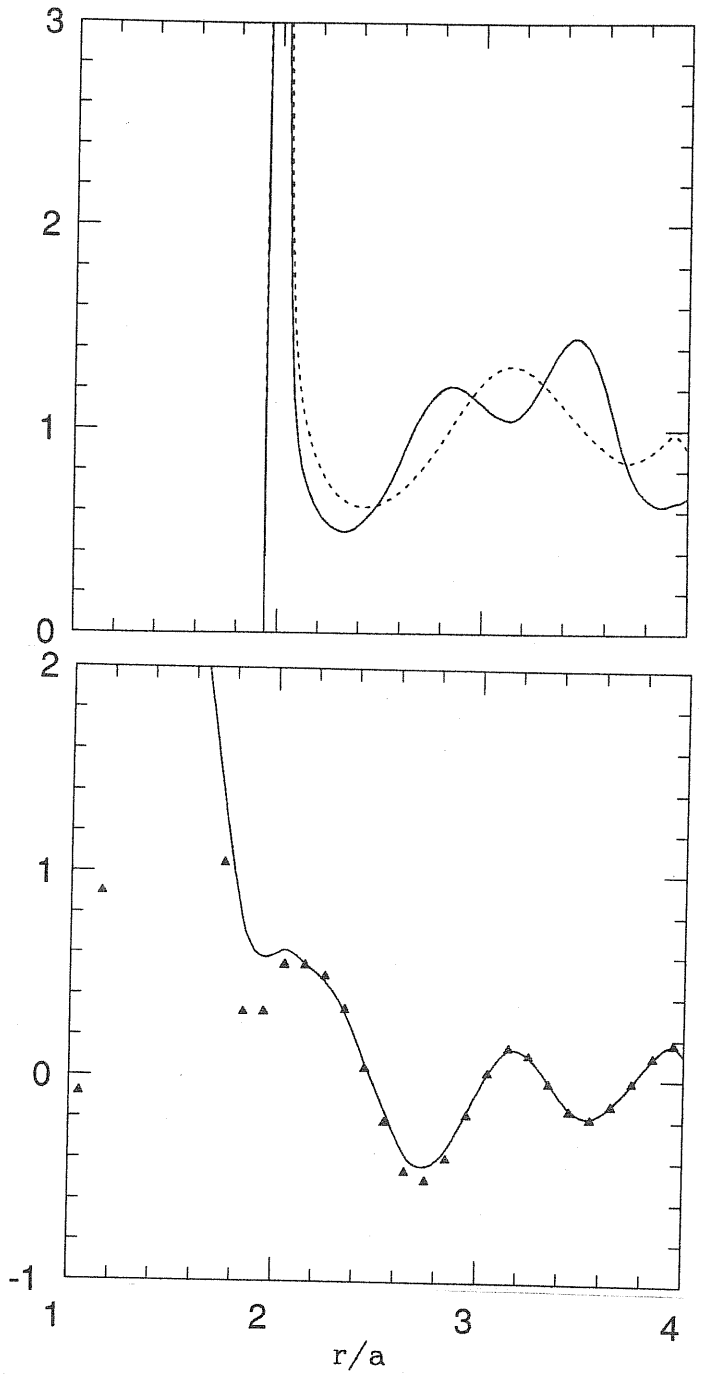

Fig. 4.12a – upper figure: pair correlation functions g_{AA} in the LAM (set 3) at $V^* = 22$; dashed line, HNC solutions; solid line, TC-IHNC solution . Lower figure: bridge functions $B^{(4)}_{AA}(r)$. Triangles, bridge calculated from the HNC solution. Solid line, cross-over bridge function obteined from it.

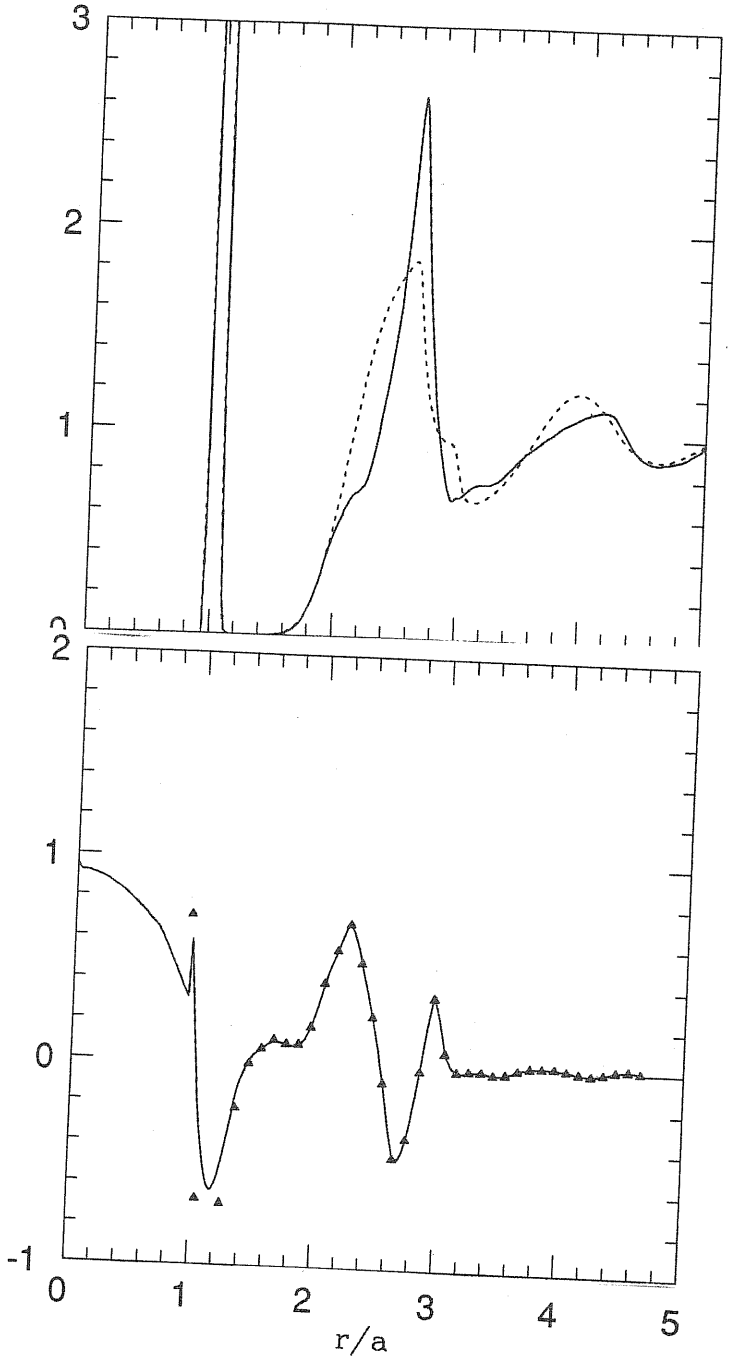

Fig. 4.12b – upper figure: pair correlation functions g_{AB} in the LAM (set 3) at $V^* = 22$; dashed line, HNC solutions; solid line, TC-IHNC solution . Lower figure: bridge functions $B^{(4)}_{AB}(r)$. Triangles, bridge calculated from the HNC solution. Solid line, cross-over bridge function obteined from it.

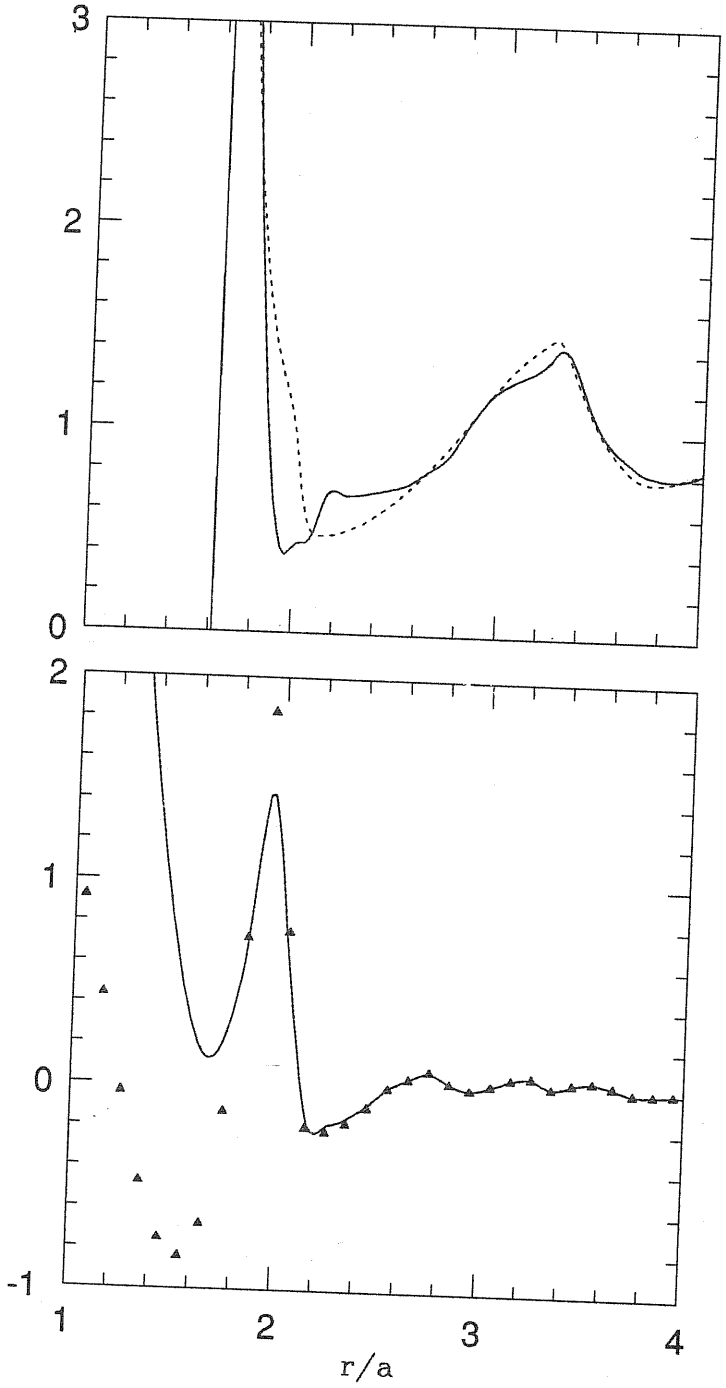

Fig. 4.12c – upper figure: pair correlation functions g_{BB} in the LAM (set 3) at $V^* = 22$; dashed line, HNC solutions; solid line, TC-IHNC solution . Lower figure: bridge functions $B^{(4)}_{BB}(r)$. Triangles, bridge calculated from the HNC solution. Solid line, cross-over bridge function obteined from it.

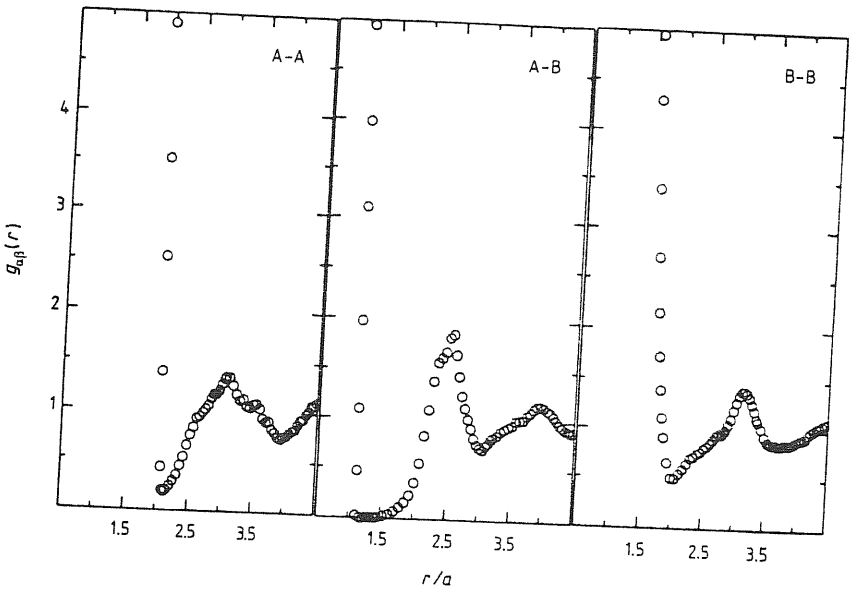

Fig. 4.13 – Partial pair distribution functions $g_{\alpha\beta}(r)$ in the LAM (set 2) at coupling $V^* = 22$ from Monte Carlo simulation.

Chapter 5

Conclusions

In this thesis we presented an elementary, primitive statistical mechanical model showing in the liquid phase both association and directionality in the interactions in a variable degree on varing the temperature, which is meant to represent in a semiclassical way the structural consequences of the incipient electronic localization process that occurs near freezing in the melts of IV group and III- IV semiconductors.

This aim was achieved introducing, in analogy with BCM used in the solid state, a Bond Particle component in addition to the atomic one, subjected to localization between two different atoms with the constraint that the maximum coordination number possible is of 4 BP around an atom, an 2 atoms around a BP. In particular we explored a representation of the model, the Localized Attraction Model, consisting essentially of a mixture non-additive hard spheres where the atomic component shows on his surface adhesion to the BP component, in the form on a narrow, spherically symmetric well. This permits to represent the characteristic fluctuations towards local tetrahedral configurations present in the liquid near freezing, due to the process of forming and breaking of covalent bonds, that was shown to be present by the recent first principle molecular dynamics simulation of Stich and Car on liquid Silicon[13]

The inclusion of the BP component permits to treat an effective directional, many body interaction between atoms by the introduction of only pair interactions between components, and allowed us to employ the formalism of standard liquid

state theory (integral equation method) to explore the structural features of the model.

We showed that this model shows quantitative agreement in describing the structure of liquid Germanium near freezing, as results from the form of the neutron scattering structure factor. A picture of a restructuring network of bonds in the liquid emerges from the model, that is similar to ideas arose in the past in the study of water. The peculiar features of the structure factor arise from correlations between atoms belonging to tetrahedral units temporary forming in the liquid. The model offers the possibility to follow the build up of a disordered network by the connection of these units on cooling, towards the formation of a disordered solid-like fourfold coordinated network structure.

This point, and the study of the effective extent of angular correlation in the melt by the examination of bond angle distribution, can be followed only in computer simulations, and constitute a point of interest for further work on the model, together with work connected to a better modelling of germanium that could be obtained substituting the hard-sphere atom-atom interaction with more realistic repulsions. The development of Monte Carlo methods to sample in an efficient way the configuration space of the primitive version of the model constitutes another point that deserves further investigations.

From the statistical mechanical point of view, we explored the accuracy of the structural prevision made by the HNC closure, and we can conclude that it is able to give semi-quantitative agreement in the liquid state up to freezing when compared with the results of a restricted set of Monte Carlo runs (made mainly in the liquid region and partially in the supercooled region). The agreement can be made quantitative in the liquid state, where the extent of angular correlation is still low, by the inclusion of appropriate bridge functions in the closure relation.

This method, even if represent a valuable tool in the exploration of the accuracy of the model, demands an higher computational effort than common algoritms for solving integral equations. Thus it should be interesting to explore the possibility of obtaining quantitative results for structure and termodynamics by means of empirically-mixed integral equations, as a fast tool in exploring the parameters of the model in the liquid state. Work is in progress in this sense with the examination of a modification of the Martynov-Sarkisov closure[5].

The accurate numerical evaluation of elementary bridge diagram for the system of interest, that involves a five-dimensional integration over functions with one very high and narrow peak, was a delicate point that required a considerable effort. It should be also interesting, from the point of view of general liquid state theory, to develop a faster algoritm to evaluate these diagrams.

It was explored, for the first time to our knowledge, the achievement of self-consistency in the determination of the elementary diagrams, by means of subsequent iterations in the solution of the integral equations, and the approximation of the first iteration commonly employed was found not to be very accurate for our model.

Moreover we showed that, connected to the increasing directionality built in in the model, the integral equation method based on the closure relation, supplemented by the elementary diagrams $B^{(4)}$ is not adequate to describe with accuracy the structural features connected to the second atomic coordination shell, in the supercooled state, and we strongly suggest that this is due to the neglection of higher order terms in the expansion of the bridge functions, due to the increasing importance of many-body correlations in the supercooled states. This strongly indicate that future investigation of the supercooled region should rely on computer simulation methods.

The model found also an application in the calculation of the possibility of freezing from the melt in a tetrahedral open structure, with consequent incresing in volume. Calculation by Badhirkan *et al.*[29] based on the density functional theory of freezing, showed that indeed it seems possible to achieve the freezing in such an open structure.

BIBLIOGRAPHY

[1] J. A. E. Desa, A. C. Wright, J. Wong, R. N. Sinclair : *J. Non-Cryst. Sol.*, **51**, 57 (1982)

[2] S. C. Moss, D. L. Price: in *Physics of disordered Materials* ,edited by D. Adler, H. Fritsche, S. R. Ovshinsky,(Plenum, N. Y.,1985), pag. 77

[3] W. Andreoni: *Helv. Phys. Acta*, **58** , 226 (1985)

[4] U. Walter, D.L. Price, S. Susman, K. J. Volin: *Phys. Rev. B*, **37**, 4232 (1988)

[5] See, for istance, S. Sugai: *Phys. Rev B*, **35** , 1345 (1987) and references therein

[6] S. Biggin, J. W. Enderby: *J. Phys. C*, **14**, 3129 (1981)

[7] O. Uemura, Y. Sagara, D. Muno, T. Satow: *J. Non-Cryst. Sol.*, **30**, 155 (1978)

[8] S. R. Elliot: *Physics of Amorphous Materials*, (Longman, London (1983)

[9] Y. Waseda, K. Suzuky: *Z. Physik B*, **20**, 339 (1975)

[10] P. S. Salmon: *J. Phys. F: Met. Phys.*, **18**, 2345 (1988)

[11] Y. Waseda: *The Structure of non crystalline Materials: Liquids and amorphous Solids* (McGraw Hill, New York,1980)

[12] C. Bergman, C. Bichara, P. Chieux, J. P. Gaspard: *J. de Phys. (Paris)*, **12**, C8-97 (1985)

[13] I. Stich, R.Car, M. Parrinello : *Phys. Rev. Lett.*, **63**, 2240 (1989) see also – I. Stich: *PhD Thesis*, (SISSA, Trieste, 1989)

[14] Q. Zhang: *PhD Thesis* (SISSA,Trieste, 1989)

[15] G. Galli, R. M. Martin, R. Car, M. Parrinello: *Phys. Rev. Lett.*, **62**, 555 (1989)

[16] see, A. Arnold, N. Mauser, J. Hafner: *J. Phys.: Cond. Matt.*, **1**, 965 (1989) and references therein

[17] W. D. Luedtke, U. Landman: *Phys. Rev B* , **37**, 4656 (1988)
– M. D. Kluge, J. R. Ray, A. Rahman: *Phys. Rev B* , **36**, 4234 (1987)

[18] P. Vashishta, R. K. Kalia, G. A. Antonio, I. Ebbsjo: *Phys. Rev. Lett.*, **62**, 1651 (1989)
– P. Vashishta, R. K. Kalia, J. P. Rino: *Phys. Rev B*, **41** , 12197 (1990)

[19] see, J. Tersoff: *Phys. Rev B*, **39**, 5566 (1989) and references therein

[20] H. Iyetomi, P. Vashishta, R. K. Kalia: *J. Phys.: Cond. Matt.*, **1**, 2103 (1989)
– P. Vashishta, R. K. Kalia, I. Ebbsjo: *Phys. Rev. B*, **39** , 6034 (1989)

[21] M. S. Wertheim: *J. Chem. Phys.*, **88**, 1145 (1988) and references therein

[22] C. G. Joslin, C. G. Gray, W. G. Chapman, K. E. Gubbins: *Mol. Phys.*, **62**, 843 (1987)
– G. J. Jackson, W. G. Chapman, K. E. Gubbins: *Mol. Phys.*, **65**, 1 (1988)
– : *Mol. Phys.*, **65**, 1057 (1988)

[23] W. R. Smith, I. Nezbeda: *J. Chem. Phys.*, **81**, 3694 (1984)
– J. Kolafa, I. Nezbeda: *Mol. Phys.*, **61**, 161 (1987)
– J. Kolafa, I. Nezbeda, Y. V. Kalyuzhnyi: *Mol. Phys.* , **68**, 1 (1989)
– I. Nezbeda, G. A. Iglesias-Silva: *Mol. Phys.*, **69**, 767 (1990)

[24] J. C. Phillips: *Covalent Bonding in Crystals and Molecules* (University of Chicago Press, Chicago Ill., 1969)
– *Bonds and Bands in Semiconductors* (Academic Press , New York ,1973) and references therein

[25] R. M. Martin: *Phys. Rev.*, **186**, 871 (1969)

[26] W. Weber: *Phys. Rev. Lett.*, **33**, 371 (1974)

– *Phys. Rev. B*, **15**, 4789 (1977)

[27] K. C. Rustagi, W. Weber: *Sol. State Comm.*, **18**, 673 (1976)

[28] A. Ferrante, M.P. Tosi: *J. Phys.: Cond. Matter*, **1**, 1679 (1989)

[29] Z. Badirkhan, A. Ferrante, M. Rovere, M. P. Tosi: *Nuovo Cimento D*, **12**, 619 (1990)

[30] J. C. Phillips : *Phys. Rev.*, **166**, 832 (1968)

– *Phys. Rev.*, **168**, 905 (1968)

[31] J. P. Walter, M.L. Cohen: *Phys. Rev. B*, **4**, 1877 (1971)

[32] O. H. Nielson, R.M. Martin: *Phys. Rev. B*, **32**, 3792 (1985)

– for experimental determination by electron scattering see: J. M. Zuo, J. C. H. Spence, M. O'Kneefe: *Phys. Rev. Lett.*, **61**, 353 (1988)

[33] U.Pietsch, V. G. Tsirelson, R. P. Ozerov: *Phys. Stat. Sol. B*, **137**, 441 (1986) see also

– C. Kittel: *Introduction to Solid State Physics*, pag 90 (4nd Ed., Wiley, New York (1971)

[34] C. M. Bertoni, V. Bartolani, C. Calandra, F. Nizzoli: *J. Phys. C*, **6**, 3612 (1973)

[35] B. G. Dick Jr., A. W. Overhauser: *Phys. Rev.*, **112**, 90 (1958)

for references about its application to the lattice dynamics of ionic systems by Cochran see Peter Brüesch: *Phonons: Theory and Experiments*, Vol.I, ch.4 (Springer, Berlin,1982)

[36] A. Fleszar, R. Resta: *Phys. Rev B*, **34**, 7140 (1986)

see also the same comparison for *GaAs* in

– L. Miglio, L. Colombo: *Physica Scripta*, **40**, 238 (1989)

[37] L. Miglio, L. Colombo: *Surf. Sci.*, **221**, 486 (1989)

– L. Miglio, L. Colombo: to appear in *Surf. Sci.* (1990)

[38] A. Goldberg, M. Batanouny, F. Wooten: *Phys. Rev B*, **26**, 6661 (1982)

– K. Winer, F. Wooten: *Phys. Stat. Sol. (b)*, **136**, 519 (1986)

[39] L. Miglio, P. Santini, P. Ruggerone, G. Benedek: *Phys. Rev. Lett.*, **62**, 3070 (1989)

– U. Harten, J. P. Toennies, Ch. Wöll, L. Miglio, P. Ruggerone, L. Colombo, G. Benedek: *Phys. Rev B*, **38**, 3305 (1988)

[40] R. G. Parr, R. F. Borkman : *J. Chem. Phys.*, **49**, 1055 (1968)

– R. G. Parr, J. E. Brown: *J. Chem. Phys.*, **49**, 4849 (1968)

[41] B. F. Levine: *Phys. Rev. Lett.*, **22**, 787 (1969)

[42] S. Go, H. Biltz, M. Cardona: *Phys. Rev. Lett.*, **34** , 580 (1975)

– K. C. Rustagi, W. Weber: *Sol. State Comm.*, **18**, 673 (1976)

[43] V. M. Glazov, S. N. Chizhevskaya, N. N. Glagoleva: *Liquid Semiconductors* (Plenum, New York, 1969)

[44] N. W. Ashcroft, D. C. Langreth: *Phys. Rev.*, **156**, 685 (1967)

[45] J. E. Enderby, D. North: *Phys. Chem. Liquids*, **1**, 1 (1968)

[46] J. P. Gabathuler, S. Steeb: *Z. Naturf.* a, **34**, 1314 (1979)

[47] P. Viscor: *J. Non-Cryst. Sol.*, **101**, 170 (1988)

[48] G. Etherington, A. C. Wright, J. T. Wentzel, J. C. Dore, J. H. Clark, R. N. Sinclair: *J. Non-Cryst. Sol.*, **48**, 265 (1982)

[49] D. Gazzillo, G. Pastore, R. Frattini: *to be published*

[50] D.Gazzillo, G. Pastore, S. Enzo: *J. Phys.: Cond. Matter*, **1**, 3469 (1989)

[51] P. Ballone, G. Pastore, J. S. Thakur, M. P. Tosi: *Physica B*, **142**, 294 (1986)

[52] Landolt-Börnstein: *Numerical Data; Group IV and III-V Semiconductors*, vol. 17a (Springer, New York, 1982)

[53] L. R. Godefroy, P. Aigrain: *Proc. Int. Conf. Physics of Semiconductors*

(Exeter), pag. 234, (1962)

[54] J. P. Hansen, I. R. McDonald: *Theory of Simple Liquids* (2nd Ed., Academic Press, London, 1986)

[55] J. M. J. van Leeuwen, J. Groeneveld, J. DeBoer: *Physica*, **25**, 792 (1959) for a systematic and detailed exposition of the diagrammatic techniques see also the article by Stell in the following ref.

[56] G. Stell, article in: *The equilibrium Theory of classical Fluids*, edited by H. L. Frisch, J. L. Lebowitz, p.II-171 (Benjamin, New York, 1964)

[57] J. K. Percus, article in: *The equilibrium Theory of classical Fluids*, edited by H. L. Frisch, J. L. Lebowitz, (Benjamin, New York, 1964)

[58] G. Stell, article in: *Phase Transitions and Critical Phenomena*, Vol 5b, edited by C.Domb, M.S. Green, p.205 (Academic, London, 1976)

[59] S.Ichimaru, H.Iyetomi, S.Tanaka: *Phys. Rep.*, **149** , 91 (1987)

[60] H.IYetomi: *Progr. on Theor. Phys.*, **71**, 427 (1984)

– L.Blum, C.Gruber, J. L. Lebowitz, P. Martin: *Phys. Rev. Lett.* , **26**, 1769 (1982)

[61] J.R.Forrest, D. A. Young: *Phys. Rev. A*, **30**, 999 (1984)

[62] J.P.Hansen, G. Zerah: *J. Chem. Phys.*, **84**, 2336 (1986)

[63] Y. Rosenfeld, N. W. Ashcroft: *Phys. Rev. A*, **20** , 1208 (1979)

[64] F. Lado: *Phys. Rev. A*, **8** 2548 (1973)

[65] S.Ichimaru, H.Iyetomi: *Phys. Rev. A*, **25**, 2434 (1982)

– *Phys. Rev. A*, **27**, 3241 (1983)

[66] P. Ballone, G. Pastore, M. P. Tosi: *J. Chem. Phys.* , **81**, 3174 (1984)

[67] S. M. Foiles, N. W. Ashcroft, L. Reatto: *J. Chem. Phys.*, **80**, 4441 (1984)

[68] M. J. Gillan: *Mol. Phys.*, **38**, 1781 (1979)

– *Mol. Phys.*, **39**, 839 (1980)

[69] P. Attard: *J. Chem. Phys.*, **91**, 3072 (1989)

[70] M.Gillan, B. Larsen, M. P. Tosi, N. H. March: *J. Phys. C: Sol. St. Phys.*, **9**, 889 (1976)

[71] J. Chirara: *J. Phys. F: Met. Phys.*, **17**, 295 (1987)

[72] P. Ballone, G. Pastore, G. Galli, D. Gazzillo: *Mol. Phys.*, **59**, 2 (1986)